ELSEVIER

Chemical Geology 210 (2004) 49–71

CHEMICAL GEOLOGY
INCLUDING
ISOTOPE GEOSCIENCE

www.elsevier.com/locate/chemgeo

Immiscible phases of magmatic fluid and their relation to Be and Mo mineralization at the Yermakovka F–Be deposit, Transbaikalia, Russia

F.G. Reyf*

Geological Institute SB, Russian Academy of Science, Sakhyanova 6a, Ulan-Ude, 670047, Russia

Abstract

Melt and fluid inclusions in minerals from the peralkaline granite intrusion and associated mineralized country rocks from the Yermakovka F–Be deposit were studied to characterize the behaviour of trace elements and exsolved fluids in the transition from magmatic to hydrothermal processes. Ore mineralization was mostly due to volatile release from a deep-seated pluton for which crystallization history and fluid exsolution can be tracked by three batches of magma (Gr1 → Gr3) intruded at the level of the ore deposition to form the Yermakovka stock. Each batch of the sequential granite group is found to intrude at decreasing temperature (from 840 to 730 °C) and progressively increasing extent of crystallization of magma in the parental pluton. This resulted in the enrichment of the ascending melts in H_2O (3.9 to 6.1 wt.%), F (2.6 to 4.1 wt.%) and some incompatible elements (Zr, Nb, Th, Rb, Pb). Although the earliest evidence for the exsolution of homogeneous fluoride–sulphate brine correlates with the final stage of the Gr2 ascent, the most intensive volatile(s) release from the emplaced magmas is shown to occur during their in situ crystallization, which was associated with the separation of exsolved fluid into immiscible phases, brine and low-salinity solution. Compositions of these fluid phases are determined using atomic emission spectroscopy of the appropriate fluid inclusions opened by a laser microprobe and EMPA and SEM–EDS analyses of daughter crystals. The brine phase is enriched in Mo, Mn, Be (up to 17, 8, and 0.3 g/kg, respectively) and contains perceptible abundances of Ce, La, Pb, Zn, whereas the low-salinity phase is enriched only in Be (up to 0.6 g/kg). The selective mobilization of the metals from the melt into fluids is considered to result from the oxidized state of the melt and fluids, peralkalinity of the melt during crystallization, and high F content of the melt. The immiscible fluid phases are shown to migrate together through the solidifying stock giving rise to the albitized granite that is enriched in molybdenite but devoid of Be minerals. In the country rocks, solutions similar to the brine and low-salinity phases of the magmatic fluid made up separate fluid flows, which produced Be and Mo mineralization and were issued predominantly from the parental pluton. Both types of mineralization are nearly monometallic which suggests that of the metals, jointly transported by the brine, only Mo and, in part, Ce and La precipitated separately at the level where the low-salinity solutions deposited Be ores.

Keywords: Granite; Magmatic fluid; Beryllium; Molybdenum; Melt and fluid inclusions

1. Introduction

Ore-grade mineralization at most granite-related hydrothermal deposits is mono- or bimetallic as if

* Tel.: +7-3012-437645; fax: +7-3012-433024.
E-mail address: felix@geo.buryatia.ru (F.G. Reyf).

0009-2541/$ - see front matter © 2004 Elsevier B.V. All rights reserved.
doi:10.1016/j.chemgeo.2004.06.004

magma-derived fluids were of a narrow specialization or, alternatively, some components of an originally multimetallic fluid precipitated selectively at different levels of a hydrothermal system. Knowledge of regularities in processes of sequestering metals by a fluid exsolved from melt is therefore of prime importance. A significant role in solving this question involves the experimental determination of the fluid/melt distribution coefficient for metals ($Di = Ci^{fluid}/Ci^{melt}$) under controlled T–P and redox conditions, depending on the composition of silicate melt and aqueous fluid. As to elements of our interest (Be, Mo), basic results have been obtained by London et al. (1988); Webster et al. (1989) and Ryabchikov et al. (1981); Candela and Holland (1984); Salova et al. (1989); Keppler and Wyllie (1991); Kravchuk et al. (1992a,b, 2000); Bai and Koster van Groos (1999), accordingly. These experiments with F-enriched peraluminous melts have revealed the D_{Be} value to be less than one within the range of temperature from 950 to 650 °C and pressure from 4 to 0.5 kbars, to decrease with increasing abundance of CO_2 in the fluid, and to display no clear dependence on Cl content of the fluid. By contrast, the experimental estimates of the D_{Mo} obtained at 1000–750 °C and 2–1 kbars vary broadly and exceed 2.0 in most cases, and they do not correlate with Cl and F content of the fluid except when the concentration of alkali halides exceeds 30 wt.% (Webster, 1997). The influence of sulphur upon D_{Be} and D_{Mo} is not yet studied experimentally, and distribution of these metals between immiscible phases of a heterogeneous fluid is scantily explored.

From melt and fluid inclusion studies, however, it follows that a natural magma-derived fluid often consists of two immiscible phases, the alkali–chloride brine and H_2O or $H_2O + CO_2$ vapor of low salinity (Roedder, 1971, 1979; Bodnar, 1995; Heinrich, 1995; Reyf, 1997 and many others). A few publications, in which metal contents of one or both immiscible phases are reported on the basis of microanalysis of individual fluid inclusions, made it clear that the heterogeneous nature of a magmatic fluid may cause the ore-forming solutions to be enriched in a severely limited number of metals (Heinrich et al., 1992; Reyf, 1997; Audetat et al., 2000). Further systematic investigations along this line are necessary to cover a more wide range of salt–aqueous systems and metals and to trace the postmagmatic history of immiscible fluid phases and their participation in the formation of ore deposits.

In this regard, investigation of the Yermakovka granite intrusion and related F–Be deposits of the same name is of special interest (Ginzburg et al., 1975, pp. 163–197; Novikova et al., 1994). The magma-derived fluid was recently found to be of an alkali–fluoride–sulphate composition which is unusual for most ore-bearing granite intrusions and hence poorly known (Reyf and Ishkov, 1999). Moreover, little if any is known about the Be contents of a magmatic fluid and hydrothermal ore-forming solutions. Unprofitable Mo mineralization occurs at the Yermakovka deposit in addition to economic Be ore.

This paper reports the peculiarities of the crystallization and degassing of the Yermakovka intrusion and the composition and behaviour of exsolved fluids at supersolidus and subsolidus conditions, based on thermometric and microanalytical studies of melt and fluid inclusions (MI and FI, respectively). It is shown that, at least late in the crystallization, the silicate melt coexisted with two immiscible fluid phases (fluoride–sulphate brine and CO_2-bearing aqueous solution of low salinity) with each being enriched in diverse metals. The immiscible fluids formed both mixed and autonomous flows which produced different types of mineralization.

2. Geology

The Yermakovka F–Be deposit is located in Western Transbaikalia, Russia, 140 km east of Ulan-Ude city (Fig. 1, Insert A), to the south of the Siberian craton. Here, Precambrian and Paleozoic metasedimentary rocks occur as a few in number, relatively small-sized (< 50 km^2) roof pendants among predominantly Paleozoic granitoids. After completion of continental collision (D–S?), the region underwent postcollision tension (C) and several stages (P_1, MZ_1, MZ_2) of intracontinental rifting (Litvinovsky et al., 2001; Yarmolyuk et al., 2001). As a result, a number of Mesozoic peralkaline granite plutons were formed within the region. One of these, referred to hereafter as the Yermakovka stock (< 0.01 km^2 at the surface),

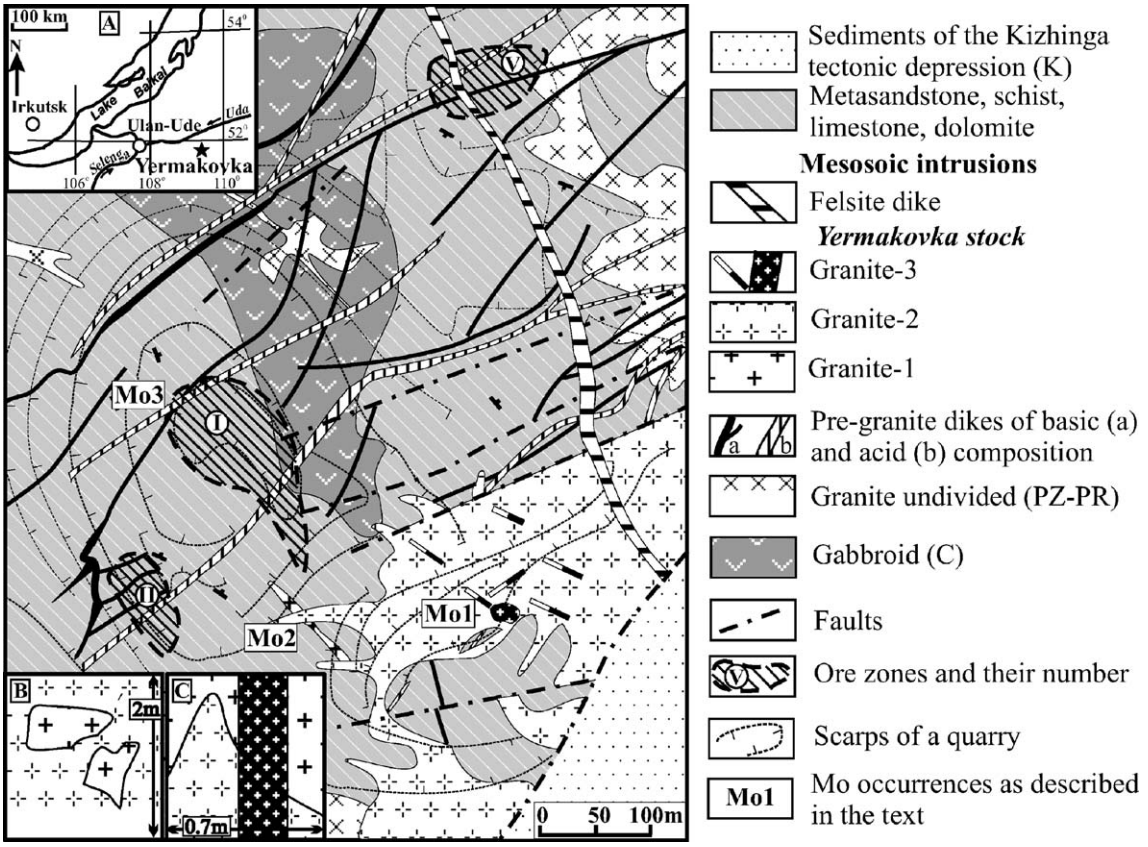

Fig. 1. Geologic sketch map of the central part of the Yermakovka deposit as documented by F.G. Reyf after quarrying with data of V.I. Galchenko and V.P. Shabanov accounted for.

is hosted by carbonate-terrigenous series rocks and is associated with the Yermakovka F–Be deposit (Fig. 1). The main orebodies are confined to limestone, they are rich in fluorite and contain bertrandite and phenakite as dominant beryllium minerals (Ginzburg et al., 1975; Novikova et al., 1994). In this respect, the deposit may be considered as a plutonic counterpart to the well-known Spor Mountain Be deposit, Utah, USA (Staatz and Griffitts, 1961; Lindsey, 1977).

2.1. Magmatism

According to crosscutting relationships observed after quarrying, magmatic rocks within the ore field formed in the succession: (1) gabbroid sill, (2) apophysal injections of amphibole–biotite granite, (3) pre-ore dike series of trachydolerite, trachyandesite, trachyrhyolite, (4) aegirine granite (Yermakovka stock, as such), and (5) postmineral dikes of felsite (Reyf and Ishkov, 1999). The recent Rb–Sr and U–Pb isotope dating has shown that these units were formed: 318 ± 2 Ma (1), 261 ± 5 Ma (2), 225 ± 5 Ma (3), 224 ± 1 Ma (4) ago, respectively; the age of ore-bearing metasomatites is 224 ± 1 Ma (Lykhin et al., 2001).

The Yermakovka stock expands with depth (Novikova et al., 1994) and is most likely to be a prominence of a deeper-seated large pluton. At the level accessible for observation, the stock was formed in three steps. The earliest granite porphyry (Gr1) occurs within metamorphic rocks as a single dike and forms diverse in size, up to several m^3, xenoliths in the younger porphyritic granite (Gr2) which occupies

more than 90% of the stock volume (Fig. 1, Insert B). Both the Gr1 and Gr2 are cut by numerous thin ($\leq$20 cm) dikes of fine- to medium-grained granite (Gr3, Fig. 1, Insert C). A small number of pegmatitic lenses and veins (Pgm) 0.1–0.4 m thick, 10–40 m in length occur in the Gr2, typically within the apical part of the stock. Centimeter-sized schlieric pegmatites are also common to some dikes of Gr3. These pegmatites are certain to originate due to the segregation of a residual melt during in situ crystallization of the emplaced Gr2 and Gr3. In the succession Gr1 → Gr3, the whole-rock composition exhibits some regular trends including increases in SiO_2, Fe_2O_3, Rb, Zr, Nb, Th and decreases in Sr and Y (Table 1). This suggests that partial separation of feldspar took place in the periods between Gr1, Gr2, and Gr3 emplacement. As compared to alkali granitoids of Transbaikalia (Zanvilevich et al., 1985), the Gr2 is more than twice enriched in F, Rb, Zr, Nb, Ni, Cu, Pb, Mn and depleted in Sr and Ba. The differences in Be, Y, and Mo are barely discernible (Fig. 2).

Quartz and perthitic alkali feldspar form roundish and euhedral phenocrysts 5–7 mm in size and are predominant minerals in the groundmass of the granites. In the inner zone of pegmatites, quartz and feldspar locally form coarse-grained aggregates or separate megacrysts (up to 6 cm in length) immersed in the fine-grained aplitic granite that constitutes marginal zones. Acicular aegirine microcrystals occur only within outer zones of some quartz phenocrysts, however, they are abundant in the groundmass quartz. As with other peralkaline granites in Transbaikalia, mesoscopic crystals of aegirine are present only in the matrix, but in this case they are usually replaced pseudomorphically by aggregates of hematite, albite, and quartz ($\pm$siderite). From Gr1 to Gr3, the abundance of aegirine in groundmass increases from 1–2% to 5%. This is also true for minor zircon, ilmenite and other sinks for trace elements (Table 2), among which monazite, ilmenorutile, and florencite largely occur in pegmatites. No beryllium minerals were found in the pegmatites and granites.

A characteristic feature of the granites is the presence of fluorite as small (20–80 μm) solid inclusions in the quartz phenocrysts (except for their core), more commonly in the groundmass quartz from the Gr1–Gr2, and as separate grains (up to 0.5 mm) in Gr3. In many cases, the quartz grains enclosing fluorite also host MI, which testifies for a magmatic origin of both. Fluorite crystals up to 3 cm in size occur within inner parts of pegmatites and often display simultaneous growth boundaries with quartz megacrysts containing MI. This suggests the fluorite crystals formed at the magmatic stage even though they do not contain inclusions of silicate melt. Many of these crystals host euhedral isotropic ralstonite-like microcrystals which display refractivity lower than that of fluorite and an EPMA-determined composition approaching $CaNa_3Mg_3Al(F_{10},OH?)$. Along the length of a pegmatite vein, the coarse-grained, fluorite-enriched aggregates are distributed unevenly, with the result that a sample weighing as much as 50–100 kg is required in order to determine the exact composition of the body as a whole. In our case, the chemical composition of the sampled pegmatite (Pgm in Table 1) characterizes only its specific part, distinctly enriched in fluorite.

2.2. Mineralization

Ore-grade Be mineralization at the deposit is presented by several fluorite-rich ledges, the largest of which are confined to limestone beds disrupted by premineral faults (Fig. 1). Being stratiform as a whole, the massive orebodies (>1 wt.% BeO) are of complex shapes in details and give way to stockwork ores (<1 wt.% BeO) which pinch out (Ginzburg et al., 1975; Novikova et al., 1994; Damdinova and Reyf, 2004). The limestone-hosted ore consists of predominant fluorite (up to 60 vol.%) and subordinate bertrandite and/or phenakite, microcline, quartz, calcite, pyrite, with sporadic galena and sphalerite. The fluorite-rich ledges hosted by aluminosilicate rocks (brecciated skarns, schists, gabbroids) are rare in occurrence, enriched in quartz, and strongly depleted in Be minerals. Ore-grade Be mineralization in granites is not found, although the abundance of Be in granites containing disseminated postmagmatic fluorite is two to four times larger than in the unaltered rocks.

Molybdenum mineralization at the Yermakovka deposit manifestes itself in diverse forms which will be referred to as Mo1, Mo2, and Mo3 mineralization (Fig. 1). Disseminated molybdenite, pyrite, and postmagmatic fluorite confined to zones of albitization in Gr2, which are irregular in shape and thickness,

Table 1
Averaged composition of the granites constituting the Yermakovka stock

Rock	Gr1		Gr2		Gr3		Pgm
N	(5)	σ	(6)	σ	(4)	σ	(1)
#SiO_2, wt.%	72.96	0.99	74.77	1.34	75.28	1.73	71.95
#TiO_2	0.30	0.05	0.30	0.05	0.32	0.03	0.36
#Al_2O_3	11.58	0.72	11.45	0.67	10.63	0.78	9.40
°Fe_2O_3	1.61	0.64	2.15	0.75	2.98	0.50	2.35
′ FeO	1.56	0.90	1.00	0.83	1.31	0.48	0.72
°MnO	0.08	0.07	0.09	0.14	0.03	0.17	0.01
°MgO	0.16	0.19	0.11	0.10	0.07	0.12	0.08
°CaO	1.34	0.46	0.60	0.37	0.43	0.35	5.40
^Na_2O	4.06	0.76	3.92	0.39	3.52	0.35	3.12
^K_2O	4.30	0.19	4.20	0.25	4.01	0.32	3.56
#P_2O_5	0.05	0.03	0.06	0.01	0.04	0.02	0.04
′ CO_2	0.57	0.67	0.36	0.29	0.17	0.36	0.16
LOI	1.73	0.73	1.13	0.46	1.13	0.39	2.60
″F	0.56	0.39	0.32	0.17	0.23	0.20	3.36
+S	<0.10		<0.10		<0.10		<0.10
Total1	100.84	0.94	100.46	0.44	100.14	0.49	103.10
Total2	100.60	0.92	100.32	0.43	100.04	0.50	101.69
ASI	0.84		0.95		0.97		0.50
°Be, ppm	7.4	2.7	5.2	2.1	6.0	2.0	5.0
^Li	57.7	46.9	23.9	22.8	23.3	20.9	27.0
^Cs	4.4	2.2	3.8	1.8	3.6	2.0	2.5
*Rb	297	68	319	45	345	40	235
*Zr	1998	711	2663	395	4493	289	1960
*Nb	117	40	158	53	325	57	105
*Th	27	10	43	22	68	20	34
*Y	113	54	94	9	90	10	435
*Sr	85	34	57	36	26	45	285
*Ba	95	65	110	102	50	118	40
*Ni	18	7	15	5	31	5	10
*Cu	9	6	12	4	5	4	19
*Zn	140	57	159	82	131	98	130
*Pb	40	7	48	25	68	25	33
*Mo	<5		<5		<5		13
Q, %normative	31.1	4.0	35.1	3.1	38.2	3.9	35.2
Or	25.9	1.1	25.2	1.5	24.1	1.9	21.7
Ab	33.9	5.7	33.6	3.4	30.2	3.3	27.2
An	1.3	2.5	1.3	0.9	1.4	1.0	1.2

(1) Gr1–Gr3 = granites in order of their emplacement.
(2) Pgm = the pegmatite vein 10 cm in thickness (together with aplitic border zones) sampled entirely.
(3) *N* = number of analyses.
(4) Total1 = sum of oxides + F.
(5) Total2 = Total1 − (O = F_2).
(6) ASI = molar ratio $Al_2O_3/(Na_2O + K_2O + CaO)$.
(7) Analytical techniques used: # = colorimetry (photometry); ° = atomic-absorption spectrometry; ′ = titration; ^ = flame emission spectrometry; ″ = potentiometry; + = gravimetric; *= X-ray fluorescence analysis.

represent Mo1 mineralization. As compared to unaltered Gr2, the albitized rocks are strongly enriched in Mo, depleted in Zr and Nb and show no difference in Be content (Table 3). The Mo2 mineralization occurs at the western apophysis of the Yermakovka stock as a network of thin quartz stringers containing subordinate fluorite and enriched in molybdenite, monazite, ilmenorutile and devoid of Be minerals. A similar

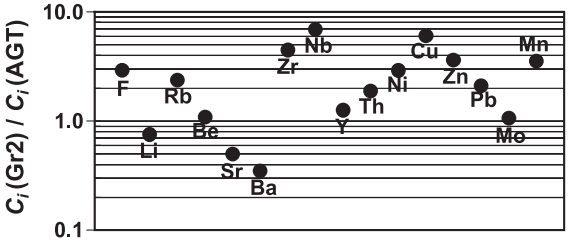

Fig. 2. Enrichment/depletion of the Gr2 in some trace elements as compared to the averaged composition of the Transbaikalian alkali granite (AGT).

network of molybdenite-rich stringers hosted by biotite schists about 300 m north west of the stock represents the Mo3 mineralization. Vein filling in this case consists of oligoclase, andradite-grossular, calcite, subordinate vesuvianite, pyrite and abundant molybdenite confined to selvages. Fluorite in the stringers is uncommon and Be minerals are not found.

Table 2
Minor granite-forming minerals as a sink for trace elements (EPMA) data, in wt.%

Mineral	Ae	Zrn	Mnz	Frc	Rt	Ilm-Rt
Rock	Gr3	Pgm	Pgm	Pgm	Gr3	Pgm
N	(3)	(6)	(2)	(1)	(2)	(2)
SiO_2	51.87	31.48	0.52	<0.24	0.21	0.12
TiO_2	1.04			0.08	96.29	86.77
Al_2O_3	0.29			28.78		
Fe_2O_3	32.76					
FeO*		0.87	0.39	0.27	2.04	4.18
MnO	0.98		0.28	0.10	0.06	0.05
MgO	0.08			<0.10		
CaO	0.41	0.09	0.12	1.00		0.02
Na_2O	12.44			<0.07		
K_2O				<0.03		
P_2O_5			29.43	26.34		<0.27
ZrO_2	0.26	64.29				0.14
HfO_2		1.47				0.67
Nb_2O_5	<0.13	0.46	1.18	0.85	2.67	8.01
Ce_2O_3		<0.17	31.18	16.53		0.08
La_2O_3		0.17	26.21	10.69		
Nd_2O_3		0.39	4.74	2.62		<0.45
Pr_2O_3		0.32	2.75	1.24		<0.38
Sm_2O_3		0.31	0.74	<0.34		<0.22
ThO_2		0.21	2.88			0.05
H_2O				11.00		
SO_3			0.24	0.31		
F			0.41	0.85		
Total	99.81	99.27	100.84	100.09	101.15	100.08

(1) Ae = aegirine, Zrn = zircon, Mnz = monazite, Frc = florencite, Rt = rutile, Ilm-Rt = ilmenorutile.
(2) N = number of analyses.
(3) FeO* = total Fe calculated as FeO.

Table 3
Change in composition of the granite-2 owing to their albitization

	Granite-2	
	Unaltered, average	Albitized, sample 177
SiO_2, wt.%	74.77	69.61
TiO_2	0.30	0.49
Al_2O_3	11.45	14.00
Fe_2O_3	2.15	0.59
FeO	1.00	1.68
MnO	0.09	0.04
MgO	0.11	0.25
CaO	0.60	1.02
Na_2O	3.92	5.45
K_2O	4.20	5.05
F	0.32	0.70
S	<0.10	0.13
Zr, ppm	2663	520
Nb	158	70
Ba	110	490
Mo	<5	190
Be	5.2	5.9

Analytical techniques used are listed in Table 1.

3. Methods

3.1. Microthermometry

A heating stage with a silicon-carbide heating element was used along with a Pt/Pt–Rh thermocouple calibrated using known melting points of seven chemically pure materials and two FI synthesized at controlled temperature and pressure. The power-law best fit of these data yields a standard error of ± 5.1 °C in the range from 112 to 1064 °C and ± 1.7 °C in the range from 150 to 350 °C. When using the heating stage, temperature cycling in the range from 100 to 350 °C was carried out to determine the homogenization temperature of fluid constituents of all preselected MI. Then temperature was raised to 580–600 °C in 30–40 min and was maintained constant over 1.5–2 h. Further heating was stepwise, with 1.5–2-h isothermal exposure after each step and a temperature increment of 50 to 20 °C depending upon the attained degree of melting of crystalline phases. Heating of MI under confining argon pressure using a

high-pressure vessel with internal heater was conducted at the Institute of Experimental Mineralogy (IEM RAS), Chernogolovka. Upon heating, pressure was raised to 5 kbar along the isochore chosen in accordance with the averaged density of a fluid constituent of the MI and then held constant during 8 to 20 h at a preselected temperature. The reverse path (along the isochore) was used when cooling, which took about 10 min and did not result in reappearance of a gas bubble or crystals.

The cooling stage is equipped with a copper/constantan thermocouple calibrated with inclusions of pure CO_2 (determined using Raman spectroscopy) homogenized in liquid at different temperatures (determined using a mercury thermometer with accuracy of ± 0.1 °C) and with solutions of known eutectic temperatures introduced into elongated cavities, abundant in some technical quartz glasses. The deviation of the data points from the exponential best fit does not exceed ± 0.2 °C in the range from $+30$ to -56 °C.

3.2. Electron microprobe analysis

Crystallized and glassed MI as well as mineral microcrystals were analyzed at the Geological Institute (GIN SB RAS), Ulan-Ude, using the analyzer MAR-3 produced by the Krasnogorsky Mechanical Plant. The samples were analyzed at 20 kV, 40 nA beam current using a spot size of 4 μm for glass and 2 to 4 μm for crystals, 10-s count time for crystals and some glassy inclusions. Most of the latter were analyzed using 25-s total count time with data collected every 5 s to account for Na loss using procedures described earlier (Kanakin et al., 1988; Reyf et al., 2000; Fig. 3). An attempt to decrease beam current was not successful since it resulted in a significant increase of random error. The accuracy of the corrected results remains unknown, however, the discrepancy between the estimated and true concentrations of Na and K seems to be insignificant in our case for the following reason. Although the loss of these elements must substantially increase the molar ratio $Al_2O_3/(Na_2O+K_2O+CaO)$, the ASI values for the analyzed MI from the Gr2 and Gr3 (0.95 and 0.82, respectively) are in agreement with the petrographic evidence that these MI were entrapped prior to and after the beginning of aegirine crystallization

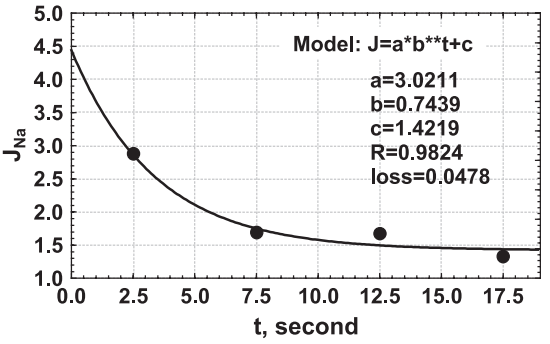

Fig. 3. The drop in the Na signal intensity ($J \approx$ wt.% Na_2O) with time (t) typical of electron-microprobe analysis of glassy MI. Values corresponding to the "zeroth" count time are believed to be the closest to the true concentrations (Gr3, MI #149).

(see Section 2.1). At the same time, the ASI values would exceed 1.0 for both the MI if our estimates of Na_2O and K_2O together were 6% and 20% lower than the corrected values for the MI from the Gr2 and Gr3. The accuracy of the EPMA technique used in this study was verified by analyzing the USNM standards 111240/52VG-2, 78854VG-568, GL-113716, Apatite 104021 and other. The differences revealed in this way were found to be insignificant at the 90% confidence level.

Daughter crystals in an opened brine inclusion were analyzed at the IGEM RAS, Moscow, using a scanning electron microscope JSM 5300 with a LINK ISIS energy-dispersion spectrometer. Recently, this inclusion was repeatedly analyzed at the GIN SB RAS, Ulan-Ude, using a scanning electron microscope LEO 1430 VP with a INCA Energy 300 energy-dispersion spectrometer at 20-kV acceleration voltage, approximately 0.5-nA current, a SATW2 entry window (these results are used in this paper). An overlay spectrum reconstruction procedure, applied to the system, was used in order to resolve S Kα line from Mo Lα and Pb Mα ones. In addition, Pb Lα lines (peaks) are detected in certain spectra (Fig. 4).

3.3. Spectroscopic determination of metal contents of fluid inclusions

A technique for atomic emission spectroscopy of individual fluid inclusions opened by a laser microprobe (AES-LM) was developed in the Geological Institute, SB RAS, Ulan-Ude and was described

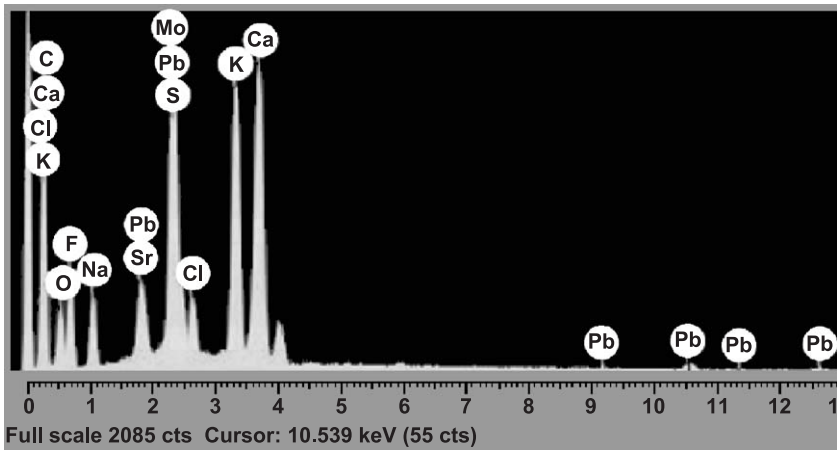

Fig. 4. The presence of Pb Lα peaks in the SEM–EDS spectrum obtained in fluid inclusions on the point 7 (see Fig. 7).

earlier (Ishkov and Reyf, 1990; Reyf, 1997). Essential features inherent in the technique are as follows:

- the mass of element rather than its concentration is determined spectroscopically to avoid the uncertainties associated with the independent estimation of the concentration of any one element (typically Na) that can serve as an internal standard;
- inclusions of the solutions slightly undersaturated in salts of interest and sealed in epoxy resin are used as standards to create an analytical curve for each element;
- the volume (V) of mineral-hosted fluid inclusions is measured using four-axis universal stage, and its total density (D) is estimated on the basis of thermometric data to calculate the FI mass ($M = V*D$) and present the results in concentration units;
- a Carl Zeiss Jena LMA-10 microanalyzer with a ruby laser was used as the basic instrument; the laser impulse energy is chosen so that it does not vaporize transparent host minerals, however, it has the capability to increase the intrainclusion pressure up to destruction of mineral layer overlying the inclusion and ejection of its contents into a spark discharge zone.

Absolute detection limits, irrespective of FI mass, are estimated to be (10^{-12} g): Na—2000, Sb—800, Pb—300, W—200, Sn—100, Zn—80, Al, Mg—50, Ni—20, Co—15, Mo, Fe, Ag—10, B—8, Mn—3, Cu—2, Be—0.1. Values of relative standard deviation for most elements lie within the interval of 20% to 30%, however, they attain 40–50% for B, Be, Cu and Mg. Concentration detection limits are calculated via dividing the absolute detection limits inherent in our device by the FI mass and therefore varies from inclusion to inclusion. Accuracy of the analyses was controlled via analysis of synthetic fluid inclusions containing solutions of known concentration of Mo, Cu and B (Ryabchikov et al., 1985; Kravchuk et al., 1992a,b; Reyf et al., 2001). As a rule, the obtained estimates are found to be less than the true values, however, the difference does not exceed the 1σ confidence interval.

3.4. Determination of the H_2O content in crystallized melt inclusions

The procedure used is based on the assumption that fluid constituents of a MI behave as isochoric system on heating up to the point of its homogenization, and its bulk density can be estimated from the measured homogenization temperature and estimated or assumed salinity. The volume and the mass of the fluid constituent can be calculated providing that the gas bubble volume and MI volume are measured using a four-axis universal stage as well as the volume of homogenized MI. The procedure and associated errors of estimation (typically $\pm 15\%$ relative at the 1σ confidence level) were described in detail earlier (Reyf et al., 2000). Because of insufficient size, none

of the MI studied via this technique were analyzed using SIMS or FTIRS. However, the water content of MI in quartz phenocrysts from the El'jurtinsky granite (the Caucasus) sampled throughout the length of the Tyrnyauz deep borehole (4.7 km) was independently estimated using the described procedure (12 samples, 35 MI; Reyf et al., 1994) and a diffusion-controlled quenching technique (10 samples, 146 MI; Thomas, 1994). Both methods yield almost the same range of values, from 2.6 to 9.8 wt.% and from 2.6 to 8.0 wt.% water, respectively. On the other hand, selected results obtained by Thomas using his diffusion-controlled quenching technique were shown to be in agreement with SIMS measurements (Thomas and Klemm, 1997). Also, as is shown in Section 4.1, our estimates of water content of MI from phenocrysts in Gr2 are in reasonable agreement with those obtained by SIMS for MI from the Ascension Island granite (Webster and Rebbert, 2001). Although this granite (AIG) is similar to the Yermakovka granite in mineralogy and chemical composition (Roedder and Coombs, 1967; Harris, 1986), the homogenization temperatures that were determined by Harris (1986) for quartz-hosted MI range from 790 to 715 °C, and the trapping temperatures for inclusions of magma-derived fluids were found to vary from 865 to 710 °C (Roedder and Coombs, 1967). These values are in excess of those obtained for the Yermakovka Gr2 (780–670 °C). Taking into account that water solubility in granite melts depends on F content (e.g. Holtz et al., 1993) and both these components decrease the liquidus and solidus temperatures in granite systems (e.g. Johannes and Holtz, 1996), the above-mentioned difference may result from lower F and/or H_2O contents in the AIG magma as compared to the Yermakovka Gr2 melt. As determined via EPMA (F) and SIMS (H_2O), the MI from AIG (sample AI-213g in the work of Webster and Rebbert, 2001) do contain lower F and H_2O abundances (1.41 ± 0.1 wt.% F against 2.6 ± 0.6 wt.%, and 4.6 ± 0.6 wt% H_2O against 5.4 ± 0.9 wt.%). In this regard, our estimates of F and H_2O contents of MI seem to be plausible.

Major and trace-element contents of the whole-rock samples are determined in the analytical laboratory of the Geological Institute SB RAS, Ulan-Ude, using the following methods and instruments: colorimetry with the photometer СФ-46 (SiO_2, TiO_2, Al_2O_3, P_2O_5); atomic-absorption spectrometry (Fe_2O_3, MnO, MgO, CaO, Be) and flame emission spectrometry (K_2O, Na_2O, Li, Rb, Cs) with the spectrometer AAS-1N; X-ray fluorescence with the spectrometer VRA-30. Accuracy of the techniques was verified via analysis of the Russia State standards СГ-3(3333-85) and СГ-1А(520-84П). The revealed differences are insignificant at the 90% confidence level. Within the range of element contents inherent in the studied rocks, relative standard deviation (%) does not exceed: for SiO_2—0.7; Al_2O_3—3.5; Fe_2O_3, LOI—7.0; Na_2O, K_2O—8.0; FeO, Zr—9.0; CaO, P_2O_5, F—12.0; MnO—17.0; TiO_2, MgO, CO_2, Rb—21.0; Nb, Zn—25.0; Be, Li, Th, Y, Sr, Ni, Cu, Pb, Mo—30.0; Ba—40.0.

4. Melt and fluid inclusions

Melt and fluid inclusions were considered to be primary provided they are confined to certain growth-zone(s) of host minerals or make up clusters distant from any healed microjoints and from surfaces of a doubly polished plate, or are single within a mineral grain. Particular emphasis has been placed on revealing the mineral sequence in order to correlate inclusions studied with a certain event and to "synchronize" inclusions hosted by diverse minerals. The porphyritic texture of Gr1 and Gr2 suggests that most of the quartz phenocrysts nucleated and grew within the deeper-seated pluton and therefore the MI from the core of the phenocrysts in these rocks provide information about changes in temperature, H_2O and F content of the crystallizing parental magma prior to the emplacement to the level observed, whereas MI in matrix quartz relate to crystallization of the emplaced magma in situ.

4.1. Melt inclusions

All MI studied occur in quartz phenocrysts and groundmass quartz and are entirely crystallized. In addition to crystalline aggregates, they contain a gaseous bubble and aqueous liquid which fills intercrystalline space being indiscernible visually (Fig. 5A). On heating, however, the gas bubble decreases in size and disappears at 160–270 °C to give the homogenization temperature for a fluid constituent of the MI. Assuming the salinity of the

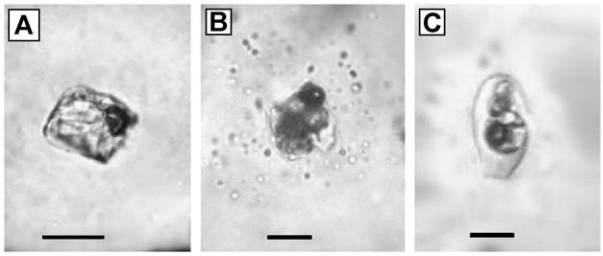

Variation in element content (wt.%) revealed by point-by-point EPMA measurements within the opened brine globule

F	42.91-0.68	FeO	28.05-13.09
SO3	56.17-4.73	MnO	13.30 - 7.23
C1	2.44-0.10	CaO	1.01 - 0.33
Na2O	17.46-3.15	P205	0.16 - 0.02
K2O	6.35-1.02		

Fig. 5. Quartz-hosted melt inclusions from the Yermakovka granite, and element concentrations of the brine globule from the remelted MI. (A) Crystallized MI without sign of postentrapment modification (Gr2, sample 113). (B) Similar MI that suffered natural decrepitation. (C) Silicate glass with globules of a brine in the inclusion remelted at 750 °C under confining argon pressure 5 kbar and then chilled (Gr2, sample 160). Scale bar length is 10 μm.

MI's fluid constituent to be about 10 wt.% equiv. NaCl (Reyf and Ishkov, 1999), the internal pressure in inclusions must exceed 5 kbars on heating up to 600 °C (e.g. Bodnar and Vityk, 1995), resulting in the decrepitation of MI prior to the beginning of melting, except for the smallest (<2 μm) MI. Several large (>15 μm) MI were therefore homogenized under a confining argon pressure of 5 kbars. The great bulk of unheated MI, however, is surrounded with numerous small FI confined to healed microjoints issuing from MI (Fig. 5B). Only a few MI display no evidence of postentrapment modification and, hence, are suitable for thermometric investigation. Moreover, some MI may have anomalous compositions if they contain accidentally entrapped microcrystals (e.g. Kfs, Fl, Aeg, Ap) that nucleated at the surface of growing host minerals. This is believed to be negligible only for the MI confined to the core of quartz phenocrysts where mineral microinclusions were not found. The microinclusions, however, are rather common in the outer parts of the phenocrysts and in groundmass quartz, so we selected (for thermometry and microanalysis) only those MI situated in the grains that are devoid of solid microinclusions. For these reasons, our thermometric and microanalytical data are rather poor (Table 4).

As can be seen from Table 4, MI hosted by groundmass quartz clearly differ in H_2O contents from those hosted by quartz phenocrysts. Moreover,

Table 4
Some features of the melt inclusions derived from thermometric and microanalytical studies

Rock	Host quartz	T_h, °C	H_2O, wt.%		F, wt.%
			Unmelted MI	Glass	
Gr1	Phenocryst	840 ± 15(6)	3.9 ± 0.8(3)	–	–
	Matrix	–	3.2 ± 0.5(1)	–	–
Gr2	Phenocryst1	780 ± 20(9)	5.4 ± 0.9(8)	5.6(1)	2.6 ± 0.6(1)
	Phenocryst2	–	7.9 ± 1.0(5)	8.8(1)	5.2 ± 0.9(1)
	Matrix	670 ± 30(8)	3.2 ± 0.5(10)	–	–
Gr3	Matrix	730 ± 20(8)	6.1 ± 0.4(6)	5.6(2)	4.1 ± 0.7(2)
Pgm	Megacryst	640 ± 10(6)	6.7 ± 0.9(4)	–	–

(1) Figure in parentheses is number of measurements.
(2) ± = standard error of a mean.
(3) – = no data.
(4) Water content of unmelted MI is estimated on the basis of joint thermometric and volumetric data using a procedure described in Reyf et al. (2000), similar estimates in homogenized (glassy) MI are taken equal to the deficit of TOTAL in appropriate electron-microprobe analyses.
(5) T_h = temperature of homogenization.
(6) F determined by EPMA.

two types of quartz phenocrysts in Gr2 contain MI that differ from each other in abundances of H_2O and F. In the case that both varieties of MI occur within a single phenocryst, those enriched in H_2O are confined to outer zones. These peculiarities argue against significant postentrapment reequilibration of the MI due to the difference in external and internal fluid pressure (e.g. Qin et al., 1992; Hall and Sterner, 1993). Also, there is indirect evidence that the MI composition does not differ significantly from that of bulk melt despite the potential presence of a boundary layer adjacent to a growing crystal that is enriched in incompatible elements. First, the analyzed apatite crystals from the pegmatite and Gr3 contain the greatest possible F abundance (3.87–4.28 wt.%) even though not all of them necessarily nucleated and grew within a boundary layer. Second, so far as all elements, excluding SiO_2, are incompatible with quartz, aegirine (among others) could nucleate at the surface of the quartz phenocrysts prior to its crystallization in the bulk melt. Nevertheless, no aegirine microcrystals were found within the quartz phenocrysts, except for in their marginal zones that grew simultaneously with the groundmass that is enriched in aegirine. On this basis, it may be assumed that the pre-intrusive evolution of the parental magma caused the enrichment of silicate melt in H_2O and F. In contrast, the H_2O content of the emplaced melt appeared to be relatively low and similar for Gr1 and Gr2. This suggests either partial remelting of phenocrysts due to a decompression of the H_2O-undersaturated magma during ascent, or partial loss of volatiles at a certain stage of the magma ascent, or both. An important observation bearing on this question is as follows. Among the MI heated under confining pressure, some are found to contain a globule(s) of brine (Fig. 5C) which did not dissolve in melt and did not decrease in size up to 850 °C. About 20 similar MI lie on a pseudosecondary trail in the quartz phenocryst from Gr2 and the relative volume of the brine globules, if present, broadly varies in the cogenetic MI which suggests the separation of the brine from silicate melt late in the ascent of this batch of magma. The enrichment of the globules in S (table in Fig. 5) poses a question of why S was not detected in the MI studied using EPMA. The question is clarified in Section 5.3.

Inasmuch as the analytical total for the glassed (homogenized) melt inclusions is less than 100%, and the difference represents a crude independent estimate of the water content of the MI, this value and the F content may be considered as the sum of volatiles that would be lost during crystallization of the preserved melt if the system were open. On these grounds, the EPMA results for MI are recalculated to obtain the composition of the crystalline product (“dry residue”) (Table 5).

When compared to the crystalline product CP 113, the average Gr2 composition is different, at the 1σ confidence level (Table 1), only regarding MnO, CaO, Na_2O, and K_2O. An elevated abundance of CaO in the granite is likely caused by the postmagmatic crystal-

Table 5
Electron microprobe analyses (in wt.%) of remelted glassy MI in comparison with calculated products of their crystallization and related granite whole-rock samples

Object	Melt inclusions		Crystalline products		Whole rocks	
Granites	Gr2	Gr3	Gr2	Gr3	Gr2(6)	Gr3(4)
MI number	113	149	113	149		
SiO_2	69.97	70.03	75.04	75.83	74.77	75.28
TiO_2	0.25	0.18	0.27	0.19	0.30	0.32
Al_2O_3	10.85	10.18	11.64	11.02	11.45	10.63
FeO*	2.85	2.47	3.06	2.67	3.15	4.29
MnO	0.31	0.24	0.33	0.25	0.09	0.03
MgO	0.08	0.07	0.09	0.07	0.11	0.07
CaO	0.09	0.02	0.10	0.02	0.60	0.43
Na_2O	4.07	4.84	4.37	5.24	3.92	3.52
K_2O	4.18	4.11	4.48	4.45	4.20	4.01
SO_3	< 0.19	< 0.19	< 0.20	< 0.20	< 0.05	< 0.05
Cl	0.29	n.d.	0.31	n.d.		
F	2.60	4.02	0.32	0.23	0.32	0.23
P_2O_5	< 0.09	0.02	< 0.09	0.02	0.06	0.04
CO_2					0.36	0.17
LOI					1.13	1.13
Total1	95.54	96.15	100.00	100.00	100.46	100.14
Total2	94.45	94.46			100.32	100.04
Δ	5.60	5.50				
Total3	92.94	92.14				
ASI	0.95	0.82	0.95	0.82	0.95	0.97

(1) FeO*= total Fe calculated as FeO.
(2) n.d. = element not determined.
(3) Total1 = sum of oxides + F.
(4) Total2 = Total1 − (O = F_2).
(5) Total3 = Total1 − F.
(6) Δ = 100 − Total2 ≅ wt.% H_2O.
(7) ASI = molar ratio $Al_2O_3/(Na_2O + K_2O + CaO)$.

lization of calcite (CO_2 is also present in Gr1–Gr3, Table 1). There is no evidence, however, that hydrothermal alteration or crystal separation might be responsible for the reduced content of MnO, Na_2O, and K_2O in the rocks (Gr2). On the other hand, these components could be removed from the melt by exsolved fluid (see further text). The foregoing is also valid for the couple CP149–Gr3.

4.2. Inclusions of a magmatic fluid (MFI)

The presence of numerous secondary fluid inclusions in rock-forming quartz presents significant difficulties for the identification of quartz-hosted MFI. Such identification, however, poses fewer problems when dealing with magmatic fluorite. First, some small fluorite grains hosted by groundmass quartz contain in turn single fluid inclusions similar to the brine globules described above (Fig. 6A and B). Second, many fluorite crystals from pegmatites host undoubtedly primary MFI confined to discrete growth-zones (Fig. 6C) or in the core of crystals (Fig. 6E). These growth-zones and clusters comprise, as a rule, two dominant types of FI of different composition (Fig. 6D and F). The brine inclusions (MFI-1) contain up to 10 daughter crystals (Fig. 6G) which occupy 46–48% of the inclusion volume thus providing a total salinity of about 70 wt.% and a bulk brine density of 1.7–2.1 g/cm^3 (Reyf and Ishkov, 1999). Semiquantitative SEM–EDS analysis of the daughters exposed in opened inclusions (Table 6) and major-element mapping (Fig. 7) have revealed a predominance of sulphates and fluorides of Na, K, and to some extent Ca. Based on the volumetric and SEM–EDS data (Table 6, Fig. 7) and taking the densities of aqueous solution (at 20 °C) and all daughter crystals to be about 1.13 g/cm^3 and 2.6 g/cm^3 (like that of Na_2SO_4), respectively, the contents of some constituents in the brine inclusion may be crudely estimated. The estimates are as follows (wt.%): S ~ 8.1, Cl ~ 0.10, Fe ~ 0.03, Mn ~ 0.05, Pb ~ 0.01, Zn ~ 0.03, Ce ~ 0.17, La ~ 0.20. Mo Lα lines were shown by the INCA Energy 300 system in some spectra (points 4, 2 and 7 in Fig. 7); however, they are detectable only at the confidence level <0.95. On heating, all large crystals in the brine inclusions dissolve at 460–480 °C prior to or after the gas bubble disappearance, whereas small

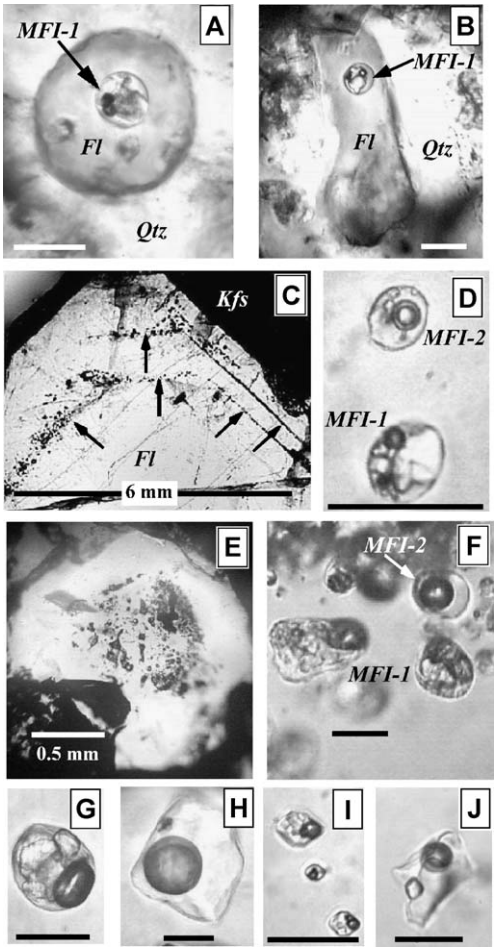

Fig. 6. Inclusions of granite-derived magmatic fluids (A–I) and ore-forming solutions responsible for the formation of the F–Be ore (J). (A, B) Primary brine inclusions (MFI-1) hosted by small fluorite grains (Fl) which in turn are included in groundmass quartz (Qtz) from aplite zone of a pegmatite (A, sample 152-2) and from Gr3 (B, sample 149); (C, D) confinement of the primary fluid inclusions to the growth-zones (arrows) of a fluorite crystal from pegmatite (C, sample 144-4) and magnified image of one of the zones containing two types of the fluid inclusions, MFI-1 and MFI-2 (D); (E, F) confinement of the primary fluid inclusions to a core of fluorite grain from a pegmatite (E, sample 37-4) and magnified image of the core displaying the coexistence of two types of inclusions, MFI-1 and MFI-2, different in composition (F); (G, H) representative fluorite-hosted inclusions of immiscible phases of the magmatic fluid: brine (G) and low-salinity CO_2-bearing solution (H); (I) quartz-hosted pseudosecondary brine inclusions similar to the MFI-1 (Pgm, sample 37-3); (J) primary inclusion of ore-forming solution in fluorite co-precipitated with phenakite (sample 130). Scale bar length is 30 μm unless otherwise noted.

Table 6
Semiquantitative SEM–EDS analyses of exposed daughter crystals (in wt.%) in the opened brine inclusions from sample 152-2

	Points of measurement in Fig. 7, SE							
	1	2	3	4	5	6	7	8
Vol	0.4	0.6	20.0	12.3	0.2	0.15	0.1	0.05
K	1.6	2.6	0.6	22.5	2.1	12.6	14.4	11.4
Rb				0.6				
Na	5.1	18.5	26.8	8.8	32.8	8.5	4.9	1.0
Ca	28.0	6.8	3.4	1.2	8.2	11.7	17.1	18.9
Sr							4.5	
Al						1.6		
Mn	0.5	0.7	0.4			16.7		
Fe						12.2		3.7
Pb							10.2	
Zn								40.0
O	10.5	25.2	23.9	49.5	11.6	5.9	18.5	2.8
S	5.3	13.6	19.8	13.6	2.4	9.7	10.4	18.9
F	5.9	13.7	12.3	3.8	9.5	19.1	17.3	3.4
Cl	0.7	3.5	12.8		33.3	2.1	2.9	
P		2.1						
Ce	16.6	7.6						
La	22.1	5.8						
Pr	1.9							
Nd	1.9							

(1) All elements analyzed, results normalised.
(2) Vol = volume% of analyzed crystals (relative to the FI volume).

transparent and opaque crystals remain to the point of inclusion decrepitation. The latter are entirely dissolved only in several small-sized MFI-1 at 600–630 °C and higher temperatures (715 °C). However, repeated heating shows an increase of the gas dissolution temperature of 240–300 °C. Therefore, the final homogenization temperature is not determined exactly but is believed to be about 600 °C. The lack of information about the positions of isochores in P–T space for such chemically complex water–salt systems gives no possibility of estimating the entrapment pressure on the basis of thermometric data.

The second type of cogenetic fluid inclusions (MFI-2) contains only two to three small crystals (about 1 vol.% each) and a gas bubble with a thin rim of liquid CO_2 (Fig. 6H, Table 7). One of the daughter crystals has high birefringence and is most likely calcite; another crystal is opaque and nonmagnetic and looks like an Fe–Mn oxide. These crystals do not dissolve at the temperature of gas bubble disappearance and instead remain to the point of inclusion decrepitation. Some inclusions are intermediate in composition between MFI-1 and MFI-2, however, they are few in number. In quartz from pegmatites, inclusions similar to MFI-1 and MFI-2 are few in number, small in size, and secondary or uncertain in origin (Fig. 6I).

It must be noted that in addition to MFI-1 and MFI-2, numerous gas inclusions (GI) occur in the fluorite crystals from pegmatites and are confined to the same growth-zones and clusters as the FI. As a rule, there are reasons to suspect these GI to originate via refilling of MFI-1 and MFI-2 with air during cutting and grinding the samples. The temperature cycling of these GI within the range from 0 to −150 °C did not reveal the appearance/disappearance of any liquid or solid phases, except for initially observed

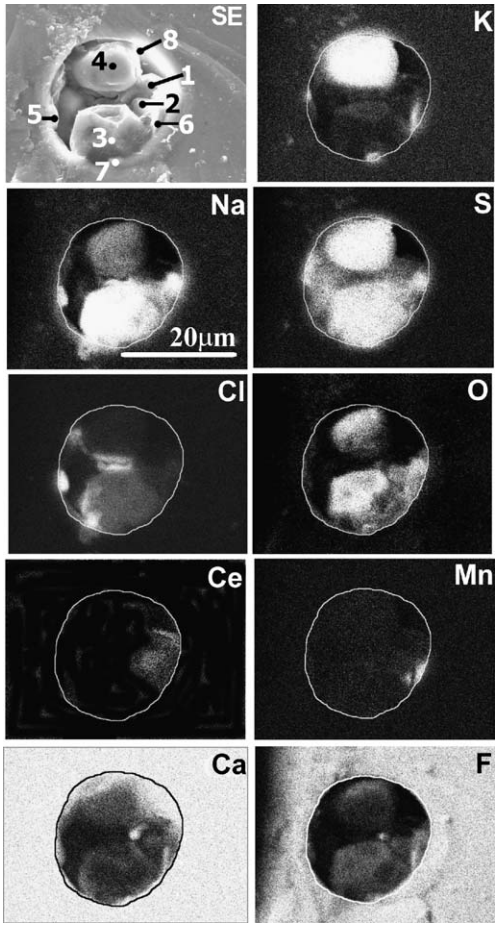

Fig. 7. Secondary electron image and selected element maps (X-ray) of an opened brine inclusion from Pgm (sample 144-4).

Table 7
Some features of fluid inclusion solutions entrapped by magmatic fluorite (MFI-2) and by ore-related fluorite (FI-A) following from low-temperature examination

Parameters	MFI-2 (Fig. 6H)	FI-A (Fig. 6J)
T_{eut}, °C	−27.7...−30.5	−21.5...−27.0
T_h*, °C	335–355	150–205
CO_2, wt.%	7.0–10.6	4.1–18.1
NaCl wt.% eq.	2.4–8.2	4.7–10.8
Density, g/cm^3	0.82–0.87	0.95–0.98

(1) T_{eut} = first melting temperature.
(2) T_h* = bubble disappearance temperature (small daughters remain).
(3) CO_2 and NaCl contents are calculated using program FLINCOR (Brown, 1989) without regard for daughter crystals of low solubility.

"daughter crystals" if present. Less than 1% of these GI, however, contain a gas bubble and liquid CO_2 with or without a visually discernible film of aqueous solution. The origin of these CO_2-rich inclusions is not yet understood.

All the above observations suggest that during in situ crystallization of Gr2 and Gr3, the release of a fluoride–sulphate brine was followed by its separation into two (or three ?) immiscible phases or by their simultaneous exsolution from a residual melt. At first glance, such examples of liquid–liquid immiscibility are unusual inasmuch as the more common product of heterogenization of a granite-derived fluid is a mixture of liquid (brine) and gaseous (vapor) phases. This problem will be considered in more detail below.

4.3. Inclusions of ore-forming solutions

Primary fluid inclusions in minerals coprecipitated with phenakite (fluorite) and molybdenite (fluorite, garnet, see Section 2.2) have been studied to compare their compositions with those of immiscible phases of the magmatic fluid described above.

A large share of fluorite from the massive F–Be ore and attendant stockwork within the first ore zone (Fig. 1) is found to precipitate from homogeneous solutions, whereas their boiling was episodic and took place at 250–290 °C and pressure of 0.6–0.7 kbars (Damdinova and Reyf, 2004). Inclusions of the homogeneous fluid (FI-A) contain a gas bubble with a rim of liquid CO_2 and a daughter crystal identified by optical features and Raman spectroscopy as calcite. The relative volume of the calcite measured using a Fedorov universal stage varies from 2% to 6% in diverse inclusion groups, however, it is constant for FI-A of a certain population (Stel'machonok and Ishkov, 2001). Except for the enlarged daughter calcite crystals, the FI-A are similar to the MFI-2 in many other respects (Table 7 and Fig. 6, compare J and H).

The albitized aegirine granite (mineralization Mo1, see Fig. 1) is enriched not only in Mo but also in F (Table 3) and contains, therefore, postmagmatic fluorite that differs from the colourless magmatic variety by its violet colour. Nevertheless, this fluorite hosts two types of cogenetic FI that are identical to the MFI-1 and MFI-2 in phase compositions (compare Figs. 8A,B and 6G,H). On heating the brine inclusions, a gas bubble and large daughter crystals dissolve at 280–330 and 460–480 °C, respectively; complete homogenization occurs at 580–640 °C. However, this leads to an increase of the bubble disappearance temperature by 200–250 °C during repeated heating.

In contrast, fluorite from the molybdenite–monazite–quartz stringers (mineralization Mo2) hosts only one type of primary FI (Fig. 8C) which is similar to the MFI-1 in the large daughter crystal dissolution temperatures (430–450 °C). They contain a smaller

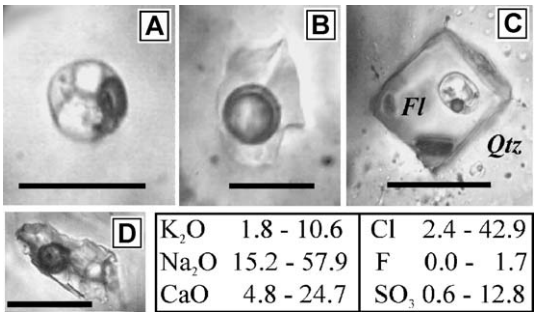

Fig. 8. Inclusions of ore-forming solutions in fluorite (A–C) and garnet (D) coprecipitated with molybdenite at the mineralized areas Mo1–Mo3 and variations in element concentration (wt.%) at diverse points of the opened inclusion (D). (A and B) Cogenetic inclusions in postmagmatic fluorite from the albitized granite (sample 143-2). (C) Brine inclusion in a small fluorite crystal from the molybdenite–monazite–quartz stringer (sample 184a). (D) Garnet-hosted brine inclusion from the molybdenite-rich calcite–garnet–oligoclase stringer (sample 188-4). Scale bar length is 20 μm. Inserted table represents the EPMA data obtained via point-by-point measurement in opened inclusion D.

gas bubble and therefore decrepitate prior to complete homogenization. Only one of the dozen inclusions studied has been homogenized at 680 °C. This value is thought to be in excess of the real homogenization temperature, which is unlikely to be higher than 580–600 °C.

In molybdenite-rich calcite–garnet–oligoclase stringers (mineralization Mo3), only andradite-grossular hosts primary or pseudosecondary FI which contain four to five daughter crystals (Fig. 8D). On heating, all the daughter crystals dissolve at 315–390 °C and the gas bubble disappears at 570–590 °C (complete homogenization). The composition of separate crystals within the inclusion opened via grinding could not be determined using EPMA, whereas point-by-point measurements (wt.%) revealed the predominance of Na-, K- and Ca-sulphates and chlorides among solids (see table in Fig. 8). The lack of F in the analyses does not necessarily mean that it is absent in the brine, because some crystal(s) could be removed while grinding. In any event, the essentially sulphate-rich composition of the inclusions is indicative of their similarity with the magmatic brine.

4.4. Metal contents of fluid inclusions

All the types of FI described, except for the garnet-hosted brine inclusions, have been analyzed using the technique of atomic emission spectroscopy with laser sampling (AES-LM). As can be seen from Table 8, metal concentrations in many FI are below the calculated detection limit which varies from inclusion to inclusion (see Section 3). With allowance made for the lowest values of the detection limit, it is apparent that metal concentrations in the FI cover 1.5–2 orders of magnitude. Nevertheless, some conclusions can be drawn on the basis of the data obtained.

Firstly, the inclusions of immiscible phases of the magmatic fluid (MFI-1 and MFI-2) are obviously distinct in their concentrations of Mo and Mn. The distinction in Be content is less apparent, however; on average, MFI-2 are enriched almost threefold in Be as compared to MFI-1. In view of the fact that MFI-1 also contain daughter crystals enriched in Ce, La, Zn and Pb (Fig. 7 and Table 6), it can be said that the magmatic brine had wider geochemical specialization relative to the low-salinity magmatic solution.

Secondly, the brine inclusions from monazite–molybdenite–quartz stringers (mineralization Mo2, see Fig. 1), although poorly presented in Table 8, appear to be similar to the brine phase of the heterogeneous magmatic fluid not only in bulk composition but also in Be, Mo and Mn content. Likewise, the compositional similarity between the low-salinity phase of the magmatic fluid and the ore-forming solutions from the first ore zone (Table 7) is corraborated by the resemblance between MFI-2 and FI-A in Be content.

Thirdly, although the concentrations of Be and Mo inherent in the magmatic fluid of the Yermakovka intrusion seem to be unusually high, they are not unique. This can be seen from Fig. 9 where the data under discussion are compared with those obtained using our technique and apparatus. However, they are related to the beryl-containing gemmiferous pegmatite from the Kukurt ore field, Pamir (K), to the Mo stockwork deposit from the Dzhida ore field, Transbaikalia (D), and the Karadub W–Sn ore field, Far East of Russia (Kd) (Stel'machonok and Ishkov, 1992; Reyf et al., 1995, 2001). In particular, as compared to the Yermakovka magmatic fluids (Y-1 and Y-2 in Fig. 9), the Kukurt pegmatite-related fluid (K) displays almost the same range of Be concentrations. The values of 0.7–1.9 g/kg were detected in several FI from the group (Kd), although Be concentrations below 0.02 g/kg are more common for the Sn-rich solutions responsible for the formation of the cassiterite deposit at the Karadub ore field (Reyf et al., 1995). Concentrations of Mo that are typical for the magmatic brine of the Yermakovka intrusion also are representative of the quartz-hosted FI from molybdenite-rich (1–6 wt.% Mo) veinlets at the Dzhida ore field (Fig. 9, analyses 62–67), whereas fluid inclusions from less mineralized (<0.5 wt.% Mo) veinlets at the same deposit (Fig. 9, analyses 68–78) show Mo contents below 1 g/kg (Stel'machonok and Ishkov, 1992). Similar to this, inclusions of magmatic brine related to the formation of the Questa Mo deposit, New Mexico, USA, and analyzed using SXRF display Mo concentrations below 1 g/kg, except for 0.99 g/kg in one of 20 FI (Cline and Vanko, 1995). Our results showing the Mo content of Sn-bearing solutions to be below 0.1 g/kg (Kd in Fig. 9) are consistent with the LA-ICP-MS data on very low Mo concentrations (0.01 g/kg) in

Table 8
Concentrations (in g/kg of solution) for selected elements in fluorite-hosted fluid inclusions determined by atomic emission spectroscopy with laser sampling

Sample no.	FI no.	Be	Mo	Mn	Fe	Cu	Al	Mg
MFI-1 from pegmatite								
115/2	68/33	0.06	1.6	1.5	1.2	<1.36	n.d.	n.d.
115/2	66/28	0.04	<0.1	<0.1	32.1*	0.05	n.d.	n.d.
115/2a	71/28	0.25	28.27	2.1	0.4	<0.01	n.d.	n.d.
115/2a	71/35	0.16	8.81	61.3	1.0	<0.01	n.d.	n.d.
144/4	71/21	0.09	5.12	1.7	0.3	<0.01	n.d.	n.d.
37/4	32/09	0.11	5.71	1.6	0.5	<0.01	n.d.	n.d.
37/4	34/11	0.04	1.38	0.2	0.1	<0.01	n.d.	n.d.
37/4	48/43	0.04	<0.17	0.9	0.8	<1.23	n.d.	n.d.
37/4	67/23	0.14	<0.40	1.4	0.5	<0.01	n.d.	n.d.
37/4	68/39	0.06	0.31	1.4	0.4	1.07	n.d.	n.d.
37/4	69/21	0.04	1.79	0.3		0.01	n.d.	n.d.
37/4	73/21	0.13	0.09	0.4	1.7	0.05	2.3	0.3
37/4	73/23	0.33	16.86	8.0	1.8	0.14	16.9	1.1
MFI-2 from pegmatite								
37/4	67/21	0.64	<0.9	<0.1	4.3	0.06	n.d.	n.d.
37/4	67/25	0.26		<0.1	<0.1	<0.02	n.d.	n.d.
37/4	67/27	0.28	<1.4	<0.2	<0.2	<0.02	n.d.	n.d.
37/4	67/29	0.33	<1.6	<0.2	<0.2	<0.03	n.d.	n.d.
37/4	68/41	0.42	2.0	1.7	10.1*	<1.88	n.d.	n.d.
37/4	69/36	0.03		<0.1	0.2	<0.01	n.d.	n.d.
37/4	69/38	0.16	0.9	0.8	5.5	<0.01	n.d.	n.d.
37/4	72/21	0.20	<0.7	<0.3	<0.2	<0.06	10.1	1.4
37/4	72/23	0.25	<0.2	<0.1	0.3	<0.01	4.6	0.3
37/4	72/25	0.08	<0.2	<0.1	<0.1	<0.02	3.0	0.4
Brine inclusions from Mnz–Mlb–Qtz stringers								
193/3	73/25	0.35	7.3	13.3	2.2	<0.03	5.5	1.0
193/3	73/27	0.46	<2.2	<0.9	<0.6	<0.09	9.9	1.8
FI-A from Phk–Kfs–Fl assemblage								
129/1	72/31	<0.23	<5.6	<2.2	<1.4	<0.49	<24.4	5.3
129/1	72/33	1.27	<2.5	<1.0	<0.6	<0.22	<10.7	3.4
129/1	72/35	<0.11	<2.7	<1.1	<0.7	<0.24	<11.9	3.2
129/1	74/25	<0.01	<0.1	<0.1	<0.1	<0.01	<0.6	0.6
129/2	76/25	<0.14	<4.6	<2.4	12.6*	0.38	<13.7	1.2
129/2	76/27	<0.34	<11.0	<5.7	<2.8	<0.33	85.4*	1.5
129/2	76/31	0.38	<2.8	<1.4	<0.7	<0.08	<8.3	0.6
129a	74/23	<0.02	<0.1	1.0	5.3	0.06	<0.9	8.1
129b	75/23	2.38	<96.0	<63.0	49.8*	<1.92	338.3*	6.9
129b	75/25	<2.42	<99.0	52.1*	<25.0	<1.98	<218.9	<3.4
129b	75/27	3.33	<146.2	<95.9	<36.9	1.74	<323.4	<5.0
129b	75/29	0.07	<29.2	<19.2	<7.4	<0.58	26.6	<1.0
129b3	75/34	<3.32	<135.7	<89.0	<34.3	<2.71	240.3*	6.9
129b3	75/36	0.42	<20.0	<13.1	<5.1	0.31	<44.3	<0.7
129b4	75/31	<0.43	<17.6	<11.5	8.6	<0.35	<38.9	1.1

Table 8 (*continued*)

Sample no.	FI no.	Be	Mo	Mn	Fe	Cu	Al	Mg
FI-A from Phk–Kfs–Fl assemblage								
129b6	75/38	0.87	<84.8		<21.4	0.84	<187.7	<2.9
129b6	75/40	1.95	<27.5	<18.1	<7.0	<0.55	<60.9	<0.9
129b6	76/23	3.31	<12.1	<6.3	<3.1	2.81	129.1*	1.7
5/22	74/21	0.22	<0.2	4.2	98.1*	0.25	12.2	7.8

(1) n.d. = element not determined.
(2) <0.1 = concentration detection limit calculated in the cases that analytical line did not emerge in a spectra (see Section 3).
(3) *= apparently abnormal values resulted from contamination by microclasts of xenogeneous material.

the W-bearing brines from the Mole Granite district, Australia (Audetat et al., 2000).

Concentrations of Cu in the brine inclusions rarely exceed 0.1 g/kg which is less than those in ore-forming solutions of the Bingham porphyry copper deposit, USA, Utah (1.2–3.7 g/kg, Vanko et al., 2001, PIXE + SXRF) and in magmatic brine of the Mole granite (0.3–2.1 g/kg, Heinrich et al., 1992, PIXE; Audetat et al., 2000, LA-ICP-MS). Both Zn and Pb are not detected spectroscopically in the inclusions studied here, but the greatest possible concentrations, although not listed in Table 8, are typically below 1 and 4 g/kg, accordingly. This is in agreement with our estimates based on volumetric and SEM–EDS data (Zn ~ 0.3 and Pb ~ 0.1 g/kg, see Section 4.3.). Much higher contents of Zn and Pb (3.2–14.6 and 2.5–7.9 g/kg, respectively) were determined by PIXE and LA-ICP-MS in inclusions of brine that exsolved from the Sn–W–F-mineralized Mole granite pluton and, in all likelihood, had a direct bearing on the formation of Pb–Zn–Cu-dominated mineralization restricted to exocontact zones of the pluton (Rankin et al., 1992; Heinrich et al., 1992; Audetat et al., 2000). Also, Pb and Zn contents in excess of 1 g/kg were detected by AES-LM in quartz-hosted FI from the Ag–Pb–Zn-dominated ore of the Banska Stiavnica deposit, Slovak Republic (Prokof'ev et al., 1992; Reyf et al., 1992).

Crude estimates of Ce and La contents in the MFI-1 that are made in Section 4.3. (~ 1.7 and ~ 2.0 g/kg, respectively) are in excess of those determined by LA-ICP-MS in brine inclusions from the Mole granite (Ce 0.001–0.017, La 0.002–0.31 g/kg, Audetat et al., 2000) and in low-salinity FI from the Huanuni tin deposit, Bolivia (La < 0.0001–0.25 g/kg, Muller et al., 2001). However, the FI of moderate salinity from the same deposit have displayed La contents of 0.33–1.07 g/kg. A crush-leach analysis of the quartz-hosted brine inclusions from the REE–Th–U-mineralized part of the Capitan Mountain granite pluton, New

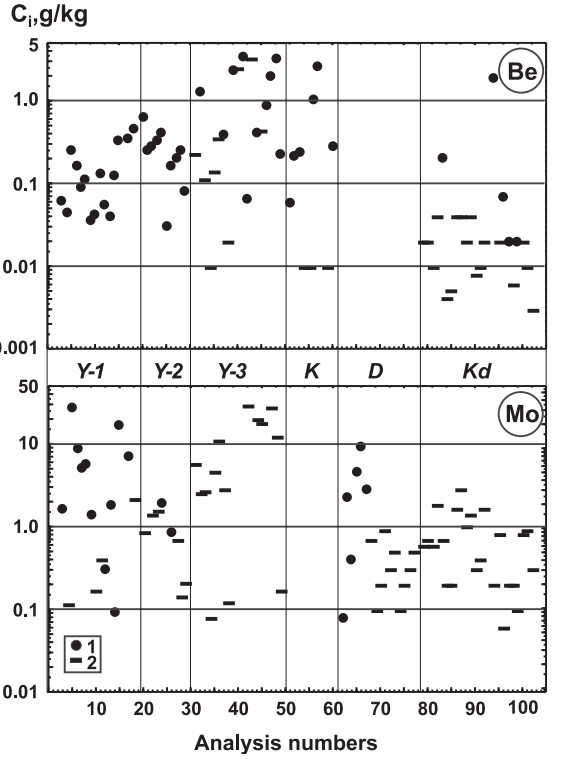

Fig. 9. Concentrations of Be and Mo in diverse fluid inclusions in comparison with data obtained in this study. Y—the Yermakovka deposit: brine (Y-1) and low-salinity (Y-2) phases of the magmatic fluid, and ore-forming solutions (Y-3) of the first ore zone; K—beryl-containing gemmiferous pegmatite, Kukurt ore field, Pamir; D—stockwork Mo deposit, Dzhida ore field, Transbaikalia; Kd—cassiterite deposit in a breccia pipe, Karadub ore field, Far East of Russia. 1 = concentration detected. 2 = detection limit calculated for the cases that elements "not detected".

Mexico, USA, is reported to contain Ce 0.08–0.58 g/kg and La 0.07–0.33 g/kg (Campbell, 1995).

Detection limits for Zr and Nb inherent in the analytical procedure used in this study are unknown. However, the magmatic fluids were undersaturated in these elements and this is evident from the decrease of Zr and Nb abundances in the Gr2 due to its albitization at subsolidus temperature (Table 3).

In as much as our results do not conflict with the relevant data obtained by PIXE and LA-ICP-MS techniques, it may be inferred that the brine phase of the heterogeneous fluid released from the Yermakovka intrusion was enriched in Mo, Be, Ce, and La to the levels inherent in the fluids that were involved in the formation of appropriate ore-grade mineralization. By contrast, Cu, Zn, and Pb contents of the brine are lower than those of solutions responsible for the production of the Cu, Zn, Pb-dominated ores. The low-salinity phase of the magma-derived fluid under study is distinctly specialized only in Be.

5. Discussion

Although the pegmatite-forming melt was shown to produce fluids compositionally similar to solutions that gave rise to the Be and Mo mineralization, some of the same fluids would be released from any part of the stock where residual melt occupied intercrystalline space. The pegmatite bodies and stock as such, however, are too small in size to make a perceptible contribution to the formation of the Yermakovka deposit that stores in excess of 10,000 tons BeO (Kremenetsky et al., 2000). This brings up the question of whether the data obtained may be applied to determining the real source of ore-forming solutions.

5.1. The use of the pegmatite as a model for the magmatic source of ore-forming fluids

It is apparent that a batch of emplaced magma and a parental pluton crystallize at diverse $P-T$ conditions and thus must traverse somewhat different paths in their geochemical evolution. According to the petrographic observation that the basic sinks for most of the minor constituents (Table 3) typically began to crystallize only after emplacement of the Gr1 and Gr2 and that the earliest evidence for fluid separation (Fig. 5C) suggests it occurred during the final stage of the Gr2 ascent, the difference in the incompatible elements between Gr1 and Gr2 is thought to reflect the evolution of the parental pluton that produced the Yermakovka stock. In all likelihood, to the point of the Gr2 emplacement, at least H_2O, Zr, and Nb were incompatible in both the parental pluton and ascending batches of magma since phenocrysts in the Gr1 and Gr2 are represented only by quartz and feldspar which do not contain perceptible concentrations of these constituents and are devoid of primary FI and microinclusions of aegirine, zircon, monazite, ilmenorutile, and rutile. Inasmuch as the enrichment of the Gr2 relative to Gr1 in these constituents is almost identical (1.38, 1.33, 1.35, respectively, see Tables 1 and 4), we can estimate the extent of crystallization for the pluton using equation for the Rayleigh-type distillation:

$$C/C_0 = R^{(k-1)},$$

where C and C_0 are current and initial element concentrations in a melt, R is the fraction of residual melt, and k is the bulk crystal/melt distribution coefficient. Taking k to be equal 0.1 for H_2O, Zr and Nb, the calculated values of R are 0.70, 0.73 and 0.72, respectively. With allowance made for about 10% of phenocrysts present in the Gr1, at least 38% of the parental melt had to be crystallized by the time of Gr2 emplacement.

Similar calculations for the Gr3 relative to the Gr1 (Tables 1 and 4) give rather ambiguous results because incipient fluid separation and the intensification of zircon and fluorite crystallization would increase k for H_2O, F, Zr to an uncertain extent. However, inasmuch as the general sinks for Nb (monazite and rutile) are met only in pegmatites, we suppose that Nb still remains incompatible ($k = 0.1$) to the point of Gr3 emplacement. If so, the calculated value of R would be equal to 0.32. Based on this value, the reverse calculation gives the values of $k = 0.61$ and 0.43 for H_2O and F, respectively, which suggests the onset of fluid separation in the parental pluton in the period between Gr2 and Gr3 emplacement.

From the above, it follows that as opposed to the Yermakovka stock, the parental pluton began to release a fluid at a higher extent of crystallization. One of the possible consequences is that the exsolved fluid would be more enriched in perfectly incompat-

ible elements such as Be and Mo (no sinks for these elements are found among magmatic minerals). In addition to that, the exsolved fluid could be homogeneous within the pluton due to elevated pressure and could separate into immiscible phases at a shallower level. Nevertheless, in our case, the general regularities in fluid separation and trace-element distribution between coexisting phases are supposed to be similar in both the deep-seated magmatic source of fluids and the emplaced batches of the parental magma.

5.2. Immiscibility in a magmatic fluid: aqueous alkali–chloride systems versus alkali–fluoride–sulphate ones

Our observation that simultaneously trapped inclusions of magmatic fluid, the MFI-1 and MFI-2, both homogenize to a liquid phase are in sharp contradiction with the more common and well-explained evidence for the separation of magmatic fluid into liquid and gaseous phases. Liquid–gas immiscibility is inherent in the systems like H_2O–NaCl (Sourirajan and Kennedy, 1962), which magmatic fluids of most granite intrusions belong to. In our case, however, the dominant components of the magmatic fluid are fluorides and sulphates of Na and K, many of which form binary aqueous systems of other type referred to as type 2 or p-Q systems (e.g. Fyfe et al., 1978). Although these systems are still poorly known, it is experimentally shown that the equilibria brine–liquid–gas and brine-supercritical fluid are possible in the ternary system, for instance with H_2O–K_2SO_4–$KLiSO_4$ (Valyashko, 1990).

Since the fluid released from the Yermakovka intrusion is much more complex in composition as compared to the above-mentioned ternary system, it is impossible to fit our fluid inclusion data to the available quantitative diagram. Instead, we use two of 11 schematic diagrams showing stable phase equilibria at certain T and P (Valyashko, 1990, p. 146). The assumed composition of the initial exsolved homogeneous brine is arbitrarily placed as a solid circle on these diagrams to interpret obtained empirical data. As can be seen from Fig. 10, a decrease of P and/or T would significantly reduce the brine field causing the initial brine data point to fall inside the three-phase field where brine and supercritical fluid (open circles in Fig. 10) would coexist with the solid

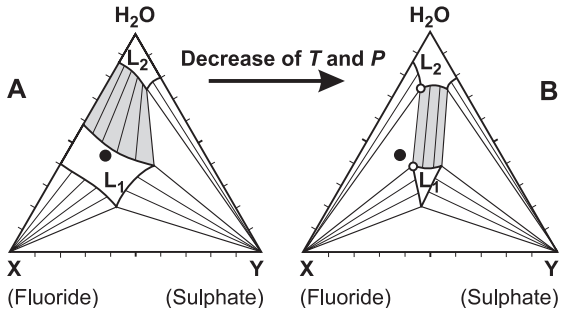

Fig. 10. Schematic diagrams showing phase equilibria in a ternary p-Q system at certain T and P decreasing from A to B, after Valyashko (1990). Fields of brine L_1 and low-salinity solution L_2 are shown not to scale; shaded area is a field of liquid immiscibility; thin lines are connodes; solid circle approximately corresponds to assumed composition of the brine globules from melt inclusions (Fig. 5C); open circles are compositions of immiscible liquid phases of the heterogenized brine.

phase X. Such a phase in our case is likely to be the ralstonite-like mineral described in Section 2.1.

It must be noted that a decrease of the S and F abundances in a melt due to fluid exsolution would shift the brine data point towards the H_2O apex of the triangle. This would entail a change-over from a homogeneous to heterogeneous state of exsolved fluid at elevated P and T (Fig. 10A) or a reduction of the brine fraction in a mixture of immiscible fluid phases (Fig. 10B). It is remarkable that although the compositions of coexisting fluid phases in this case would remain constant, if P and T decrease insignificantly, a bulk composition of exsolved fluid would become increasingly more depleted in salt components. The effect of CO_2 on phase relations in a p-Q ternary type system is unknown; however, by analogy with the well-studied system H_2O–NaCl–CO_2 (Pichavant et al., 1982; Frantz et al., 1992), further separation of the low-salinity solution into immiscible CO_2-rich and CO_2-poor fluids seems to be probable at low (<1 kbar) pressure.

5.3. Selective mobilization of trace elements into magmatic fluid and their separate precipitation at subsolidus temperature

When compared to the Transbaikalian Permian–Triassic alkali granites not associated with ore deposits, the Yermakovka granites are shown to be signif-

icantly enriched in F, Rb, Zr, Nb, Ni, Cu, Zn, Mn, depleted in Sr, Ba and indiscernible in Be, Y, Mo (Fig. 2). Nevertheless, the exsolved fluid is distinctly enriched only in F, S, Be, Mo and Mn (Table 8). Below, we show that in light of available experimental data, such well-marked selective mobilization of elements from the melt into exsolved fluid(s) may be largely caused by the specific redox state of the magmatic system, by the low solubility of S in silicate melts, by the predominance of Na, K, and Ca over Al in the magma, and by high F contents of the melt.

The oxidizing conditions have manifested themselves in the fact that the major carrier of Fe in the granites is presented by aegirine ($NaFe^{3+}[Si_2O_6]$), and sulphur in the inclusions of magma-derived brine occurs as sulphate ion (Fig. 7). This suggests that Mo in the melt also had a valence of six and therefore could not precipitate from the melt as molybdenite. On the other hand, molybdate species are prevalent in silicate melts at similar conditions (Candela and Bouton, 1990; Holtzheid et al., 1994) and Na- and K-molybdate complexes are expected to dominate in oxidized fluids (Kudrin, 1989; Webster, 1997). The preferential mobilization of Mo in the brine phase therefore may be determined by higher activities of Na and K as compared to the CO_2-bearing, low-salinity immiscible phase. Moreover, the addition of CO_2 reduces the fluid/melt distribution coefficients for most metals (Webster et al., 1989). The behaviour of Mn defies explanation. However, it is probable that due to oxidizing conditions, it could not exist in divalent form, it was enriched in the melt with the progress in crystallization and then was extracted by the brine (Table 8) as Na- or K-manganate.

Although the sulphur content of the melt remains unknown, the EPMA data suggest it to be below 0.2 wt.% SO_3 (Table 5), which is less than the estimated SO_3 content of the natural oxidized magmas saturated in anhydrite (0.22–0.62 wt.% SO_3, Baker and Rutherford, 1996). A thermodynamic model of Wallace, calibrated for dacitic and rhyolitic melts from 780 to 900 °C, 2–4 kbar, ΔNNO from +0.5 to +2.6, and 30–1400 ppm dissolved S, predicts that the weight ratio S(vapor)/S(melt) approaches 1000 at 750–780 °C (Wallace, 2002). Assuming the brine inclusions studied contain about 10 wt.% S (see Section 4.2.), the melt in equilibrium with such a brine would contain about 0.01 wt.% S (0.025 wt.% SO_3). This is lower than the detection limit for S (about 0.06 wt.%) inherent in the electron-probe analyzer used in this work. In view of this fact and based on available solubility data for SO_3 (Carroll and Rutherford, 1987; Luhr, 1990; Baker and Rutherford, 1996), it may be inferred that the Yermakovka granite melt could not contain SO_3 far in excess of 0.01 wt.% at $T < 750$ °C, and SO_3-containing fluid therefore would exsolve from the melt at some stage of magma crystallization in spite of the low initial S content.

The occurrence of aegirine in the Yermakovka granites and relatively low molar ratio Al/(Na + K + Ca) in the melt inclusions (ASI = 0.95–0.82, see Table 5) both attest that the melt was peralkaline in the course of the fluid exsolution. At such conditions, the fluid/melt distribution coefficients for Pb and Zn were shown to be less than unity and about two orders of magnitude lower than those in slightly peraluminous melts (Urabe, 1985). This may explain why these metals were not extracted effectively by the exsolved fluid(s) in our case. In addition, the peralkalinity of the melt, in all likelihood, prevented crystallization of beryllium aluminosilicates such as beryl and, hence, provided the accumulation of Be in residual melt over the level required for saturation of peraluminous melts in beryl (≤0.03 wt.% BeO at $T < 750$ °C; Evensen et al., 1999).

Although the fluid/melt distribution coefficient for F is less than one until F content of mildly peraluminous melt attains 8 wt.%, the D_F value would be close to 0.4, if the melt contains 4 wt% F at 800 °C, 2000 bars (Webster, 1990). The same value was obtained at 650 °C, 2000 bars for the peraluminous rhyolitic melt (London et al., 1988). Hence, the observed increase of F concentration in melt with the progress in crystallization (Table 4) suggests that the fluid(s) exsolved from residual melts would contain at least 1.6% of F. This has a direct relationship to the mobilization of Be into fluids because beryllium-fluoride complexes (BeF_3^- and BeF_4^{2-}) are the most soluble in near-neutral F-rich solutions (Wood, 1992). In the case that the exsolved fluid breaks up into immiscible phases and one of them is enriched in CO_2, the latter would be somewhat depleted in F as compared to CO_2-free phase (Webster, 1990). In the presence of CO_2, however, the fluoride-carbonate complex $BeCO_3F^-$ can occur, whose solubility is almost two orders of magnitude higher than those of the above-

mentioned fluoride complexes (Wood, 1992). In this context, the minor although discernible distinction in Be content between the immiscible fluids under discussion seems to be well explained.

Irrespective of whether the explanations given are valid or not, it seems evident that the trace elements available in the magma were sequestered by the fluid phases selectively, and two immiscible fluids different in ore specialization were issued simultaneously from the same intrusion. Both fluids are found to migrate jointly through the solidifying Yermakovka stock during formation of the albitized granites (Fig. 8A and B), however, they gave rise to separate fluid flows in metasedimentary country rocks. The most probable reason for such separation is the significant difference in densities of the immiscible fluid phases (1.7–2.1 and 0.82–0.87 g/cm^3) and, perhaps, in their rheologic properties. This assumption is in agreement with the observation of previous investigators that "molybdenite… occurs mainly below the levels of (Be) ore zones, being confined to granite dikes and apophyses" (Ginzburg et al., 1975, p. 182).

It is beyond the scope of this paper to review the factors responsible for the precipitation of metals jointly transported by the magmatic fluids. Nevertheless, an important point is that the brine containing elevated abundances of Mo, Mn, Be, Ce, and La deposited only Mo (Mo1 and Mo3 in Fig. 1) or Mo, Ce, La (Mo2 in Fig. 1) at the observable level, whereas Mn and Be precipitated at diverse levels. This fact exemplifies the formation of essentially monometallic (Mo) mineralization due to selective metal deposition from multimetallic fluids, as opposed to the almost monometallic style of Be mineralization which is caused by the narrow specialization of the low-salinity ore-forming solutions.

Acknowledgements

I appreciate the assistance of N. Karmanov, S. Kanakin (GIN, Ulan-Ude), and M. Lapina (IGEM, Moscow) in EPMA and SEM–EDS studies as well as the participation of L. Reyf in volumetry of melt inclusions and estimation of their H_2O content. Yu.M. Ishkov, one of the developers of the AES-LM technique, is acknowledged for the analysis of fluid inclusions. I thank T. Salova (IEM, Chernogolovka), whose experimental equipment was used, in part, to heat the melt inclusions under confining gas pressure, and B. Litvinovsky for reading and discussing earlier versions of the manuscript. I am especially grateful to J. Webster, G. Morgan, and A. Audetat for the thoughtful and detailed reviews. This research was supported by the Russian Foundation of Base Research (RFBR grants 00-05-64323 and 03-05-64857). This is also a contribution to the SB RAS project # 64. **[SG]**

References

Audetat, A., Gunther, D., Heinrich, C.A., 2000. Magmatic-hydrothermal evolution in a fractionating granite: a microchemical study of the Sn–W–F-mineralized Mole granite (Australia). Geochim. Cosmochim. Acta 64, 3373–3393.

Bai, T.B., Koster van Groos, A.F., 1999. The distribution of Na, K, Rb, Sr, Al, Ge, Cu, W, Mo, La, and Ce between granitic melts and coexisting aqueous fluids. Geochim. Cosmochim. Acta 63, 1117–1131.

Baker, L.L., Rutherford, M.J., 1996. Crystallization of anhydrite-bearing magmas. Trans. R. Soc. Edinb. Earth Sci. 87, 243–250.

Bodnar, R.J., 1995. Fluid-inclusion evidence for a magmatic source for metal in porphyry copper deposits. In: Thompson, J.F.H. (Ed.), Magmas, Fluids, and Ore Deposits. Mineral. Assoc. Can., Short Course Ser. 23, 139–152.

Bodnar, R.J., Vityk, M.O., 1995. Interpretation of microthermometric data for H_2O-NaCl fluid inclusions. In: Vivo, B.D., Frezzotti, M.L. (Eds.), Fluid Inclusions in Minerals: Methods and Applications. Virginia Tech, Blacksburg, pp. 117–130.

Brown, P.E., 1989. FLINCOR: a microcomputer program for the reduction and investigation of fluid-inclusion data. Am. Mineral. 74, 1390–1393.

Campbell, A.R., 1995. The evolution of a magmatic fluid: a case history from the Capitan Mountains, New Mexico. In: Thompson, J.F.H. (Ed.), Magmas, Fluids, and Ore Deposits. Mineral. Assoc. Can., Short Course Ser. vol. 23, pp. 291–308.

Candela, P.A., Bouton, S.L., 1990. The influence of oxygen fugacity on tungsten and molybdenum partitioning between silicate melts and ilmenite. Econ. Geol. 85, 633–640.

Candela, P.A., Holland, H.D., 1984. The partitioning of copper and molybdenum between silicate melts and aqueous fluids. Geochim. Cosmochim. Acta 48, 373–380.

Carroll, M., Rutherford, M.J., 1987. The stability of igneous anhydrite: experimental results and implications for sulfur behavior in the 1982 El Chichon trachyandesite and other evolved magmas. J. Petrol. 28, 781–801.

Cline, J.S., Vanko, D.A., 1995. Magmatically generated saline brines related to molybdenum at Questa, New Mexico, USA-Thompson, J.F.H. (Ed.), Magmas, Fluids, and Ore Deposits. Mineral. Assoc. Can., Short Course Ser. vol. 23, pp. 153–174.

Damdinova, L.B., Reyf, F.G., 2004. Peculiarities of the formation of diverse stockwork beryllium mineralization at the Yermakovka F–Be deposit (West Transbaikalia). Russ. Geol. Geophys. 45 (8), 43–55.

Evensen, J.M., London, D., Wendlandt, R.F., 1999. Solubility and stability of beryl in granitic melts. Am. Mineral. 84, 733–745.

Frantz, J.D., Popp, R.K., Hoering, T.C., 1992. The compositional limits of fluid immiscibility in the system H_2O–NaCl–CO_2 as determined with the use of synthetic fluid inclusions in conjunction with mass spectrometry. Chem. Geol. 98, 237–255.

Fyfe, W.S., Price, N.J., Thompson, A.B., 1978. Fluids in the Earth's Crust Elsever, Amsterdam. 435 pp.

Ginzburg, A.I., Zabolotnaya, N.P., Kupriyanova, I.I., Novikova, M.I., Shatskaya, V.T., Shpanov, E.P., Shuriga, T.N., Getmanskaya, T.I., 1975. Genetic Types of Hydrothermal Deposits of Beryllium Nedra, Moscow, USSR. 248 pp. (in Russian).

Hall, D.L., Sterner, S.M., 1993. Preferential water loss from synthetic fluid inclusions. Contrib. Mineral. Petrol. 114, 489–500.

Harris, C., 1986. A quantitative study of magmatic inclusions in the plutonic ejecta of Ascension Island. J. Petrol. 27, 251–276.

Heinrich, C.A., 1995. Geochemical evolution and hydrothermal mineral deposition in Sn (-W-base metal) and other granite-related ore systems: some conclusions from Australian examples-Thompson, J.F.H. (Ed.), Magmas, Fluids, and Ore Deposits. Mineral. Assoc. Can., Short Course Ser. vol. 23, pp. 203–220.

Heinrich, C.A., Ryan, C.G., Mernagh, T.P., Eadington, P.J., 1992. Segregation of ore metals between magmatic brine and vapor: a fluid inclusion study using PIXE microanalysis. Econ. Geol. 87, 1566–1583.

Holtz, F., Dingwell, D.B., Behrens, H., 1993. Effects of F, B_2O_3 and P_2O_5 on the solubility of water in haplogranite melts compared to natural silicate melts. Contrib. Mineral. Petrol. 113, 492–501.

Holtzheid, A., Borison, B., Palme, H., 1994. Solubilities of Ni, Co, and Mo in silicate melts. Geochim. Cosmochim. Acta 58, 1975–1981.

Ishkov, Yu.M., Reyf, F.G., 1990. Laser-Spectral Analysis of Ore-Bearing Fluid Inclusions in Minerals Nauka, Novosibirsk, USSR. 93 pp. (in Russian).

Johannes, W., Holtz, F., 1996. Petrogenesis and Experimental Petrology of Granitic Rocks Springer-Verlag, Berlin. 335 pp.

Kanakin, S.V., Reyf, F.G., Firsov, A.P., 1988. On the procedure of electron probe analysis of the felsic melt inclusions in minerals. Geol. Geophys. 10, 75–80 (in Russian, with English Abstr).

Keppler, H., Wyllie, P.J., 1991. Partitioning of Cu, Sn, Mo, W, U, and Th between melt and aqueous fluid in the systems haplogranite–H_2O–HCl and haplogranite–H_2O–HF. Contrib. Mineral. Petrol. 109, 139–150.

Kravchuk, I.F., Malinin, S.D., Chjao, B., Lebedev, E.B., 1992a. The molybdenum distribution between phases in the system fluid-granodiorite melt under 1000 °C and 2 and 4 kbars. Geokhimiya 1, 123–127 (in Russian, with English Abstr.).

Kravchuk, I.F., Reyf, F.G., Malinin, S.D., Ishkov, Yu.M., Naumov, V.B., 1992b. Investigation of Cu and Zn distribution between phases of heterogeneous NaCl–H_2O fluid using synthetic fluid inclusions. Geokhimiya 5, 735–738 (in Russian, with English Abstr).

Kravchuk, I.F., Malinin, S.D., Senin, V.G., Dernov-Pegarev, V.F., 2000. Molybdenum partition between melts of natural and synthetic aluminosilicates and aqueous–salt fluids. Geochem. Int. 38, 130–137.

Kremenetsky, A.A., Beskin, S.M., Lehmann, B., Seltman, R., 2000. Economic geology of granite-related ore deposits of Russia and other FSU countries: an overview. In: Kremenetsky, A.A., Lehmann, B., Seltman, R. (Eds.), Ore-Bearing Granites of Russia and Adjacent Countries. IMGRE, Moscow, Russia, pp. 3–56.

Kudrin, A.V., 1989. Behaviour of molybdenum in aqueous solutions of sodium and potassium chlorides at 300 to 450 °C. Geokhimiya 1, 99–112 (in Russian, with English Abstr).

Lindsey, D.A., 1977. Epithermal beryllium deposits in water-laid tuff, western Utah. Econ. Geol. 72, 219–232.

Litvinovsky, B.A., Yarmolyuk, V.V., Vorontsov, A.A., Zhuravlev, D.V., Posokhov, V.F., Sandimirova, G.P., Kuz'min, D.V., 2001. Late Triassic stage of the Mongolian–Transbaikalian alkali-granitoid province formation: data on isotope-geochemical studies. Russ. Geol. Geophys. 42, 445–455.

London, D., Hervig, R.L., Morgan VI, G.B. 1988. Melt-vapor solubilities and elemental partitioning in peraluminous granite–pegmatite systems: experimental results with Macusani glass at 200 MPa. Contrib. Mineral. Petrol. 99, 360–373.

Luhr, J.F., 1990. Experimental phase relations of water- and sulfur-saturated arc magmas and the 1982 eruptions of El Chichon volcano. J. Petrol. 31, 1071–1114.

Lykhin, D.A., Kostitsyn, Yu.A., Kovalenko, V.I., Yarmolyuk, V.V., Sal'nikova, E.B., Kotov, A.B., Kovach, V.P., Ripp, G.S., 2001. Ore-bearing magmatism at the Ermakov beryllium deposit in the Western Transbaikal region: age, magma sources, and relationships to ore mineralization. Geol. Ore Depos. 43, 46–63.

Muller, B., Frischknecht, R., Seward, T.M., Heinrich, C.A., Gallegos, W.C., 2001. A fluid inclusion reconnaissance study of the Huanuni tin deposit (Bolivia), using LA-ICP-MS micro-analysis. Miner. Depos. 36, 680–688.

Novikova, M.I., Shpanov, E.P., Kupriynova, I.I., 1994. Petrography of the ermakovsk beryllium deposit (Western Transbaikal Region). Petrology 2, 98–109.

Pichavant, M., Ramboz, C., Weisbrod, A., 1982. Fluid immiscibility in natural processes: use and misuse of fluid inclusion data: 1. Phase equilibria analysis—a theoretical and geometrical approach. Chem. Geol. 37, 1–27.

Prokof'ev, V.Yu., Reyf, F.G., Ishkov, Yu.M., Kovalenker, V.A., 1992. Metal contents of ore-forming fluids of the gold–silver–base metallic Banska Stiavnica deposit, Slovak Republic. Dokl. Akad. Nauk 324, 425–429 (in Russian).

Qin, Z., Lu, F., Anderson Jr., A.T. 1992. Diffusive reequilibration of melt and fluid inclusions. Am. Mineral. 77, 565–576.

Rankin, A.H., Ramsey, M.H., Coles, B., Van Langevelde, F., Thomas, C.R., 1992. The composition of hypersaline, iron-rich granitic fluids based on laser-ICP and Synchrotron-XRF microprobe analysis of individual fluid inclusions in topaz, Mole granite, eastern Australia. Geochim. Cosmochim. Acta 56, 67–79.

Reyf, F.G., 1997. Direct evolution of W-rich brines from crystallizing melt within the Mariktikan granite pluton, west Transbaikalia. Miner. Depos. 32, 475–490.

Reyf, F.G., Ishkov, Yu.M., 1999. Be-bearing sulfate-fluoride brine: a product of residual pegmatite distillation in an alkali granite intrusion, Yermakovka F–Be deposit, Transbaikalia. Geochem. Int. 10, 985–999.

Reyf, F.G., Prokof'ev, V.Yu., Borovikov, A.A., Borisenko, A.C., Stel'machonok, K.Z., Pakhomova, V.A., Smirnov, S.Z., Bakumenko, I.T., Gimon, V.O., Berzina, A.P., Stepanov, S.N., Kurmushin, V.A., Karpukhina, V.S., Ishkov, Yu.M., 1992. On metal contents of ore-forming solutions. Dokl. Akad. Nauk 325, 585–589 (in Russian).

Reyf, F.G., Kremenetsky, A.A., Udod, N.I., 1994. On the rest magma chamber of the El'jurtinsky granite pluton bored by Tyrnyauz deep borehole. Geochem. Int. 10, 23–33.

Reyf, F.G., Pakhomova, V.A., Ishkov, Yu.M., Demashev, S.B., 1995. The role of highly metalliferous solutions in the formation of the Verkhneye tin deposit, Karadube orefield. Geochem. Int. 32, 58–76.

Reyf, F.G., Seltmann, R., Zaraisky, G.P., 2000. The role of magmatic processes in the formation of banded Li,F-enriched granites from the Orlovka tantalum deposit, Transbaikalia, Russia: microthermometric evidence. Can. Mineral. 38, 915–936.

Reyf, F.G., Prokof'ev, V.Yu., Balitsky, V.S., Ishkov, Yu.M., Peretyazhko, I.S., Zagorsky, V.E., Smirnov, S.Z., 2001. Comparison of thermometric and spectroscopic estimates of the Boron concentrations in synthetic and natural fluid inclusions. In: Mel'nikov, F.P., Polyansky, E.V. (Eds.), Proceedings of the X International Conference on Thermobarogeochemistry. VNII-SIMS, Alexandrov, pp. 3–17 (in Russian, with English Abstr.).

Roedder, E., 1971. Fluid inclusion studies on the porphyry-type ore deposits at Bingham, Utah, Butte, Montana, and Climax, Colorado. Econ. Geol. 66, 98–120.

Roedder, E., 1979. Origin and significance of magmatic inclusions. Bull. Mineral. 102, 487–510.

Roedder, E., Coombs, D.S., 1967. Immiscibility in granitic melts, indicated by fluid inclusions in ejected granitic blocks from Ascension Island. J. Petrol. 8, 417–451.

Ryabchikov, I.D., Rekharsky, V.I., Kudrin, A.B., 1981. Mobilization of molybdenum by magmatic fluids during crystallization of granitic melts. Geochem. Int. 18, 183–186.

Ryabchikov, I.D., Reyf, F.G., Orlova, G.P., Ishkov, Yu.M., 1985. On metal content of hydrotherms in connection with the results of laser-spectral analysis of fluid inclusions. Geol. Rudn. Mestorozhd. 1, 102–105 (in Russian).

Salova, T.P., Orlova, G.P., Kravchuk, I.F., Epelbaum, M.B., Ryabchikov, I.D., Malinin, S.D., 1989. On experimental determination of the partition coefficient for molybdenum between silicate melt and salt–aqueous fluid. Geochimiya 2, 25–30 (in Russian, with English Abstr).

Sourirajan, S., Kennedy, G.C., 1962. The system H_2O–NaCl at elevated temperatures and pressures. Am. J. Sci. 260, 115–141.

Staatz, M.H., Griffitts, W.R., 1961. Beryllium-bearing tuff in the Thomas Range, Juab County, Utah. Econ. Geol. 56, 946–950.

Stel'machonok, K.Z., Ishkov, Yu.M., 1992. Influence of ore-forming solution metal contents upon molybdenum concentration in ores of the granite-derived deposit. Dokl. Akad. Nauk 325, 818–822 (in Russian).

Stel'machonok, K.Z., Ishkov, Yu.M., 2001. Metal content of ore-forming solutions of the Ermakovka beryllium deposit (Western Transbaikalia). Russ. Geol. Geophys. 42, 759–772.

Thomas, R., 1994. Estimation of the viscosity and the water content of silicate melts from melt inclusion data. Eur. J. Mineral. 6, 511–535.

Thomas, R., Klemm, W., 1997. Microthermometry study of silicate melt inclusions in Variscan granites from SE Germany: volatile contents and entrapment conditions. J. Petrol. 38, 1753–1765.

Urabe, T., 1985. Aluminous granite as a source magma of hydrothermal ore deposits: an experimental study. Econ. Geol. 80, 148–157.

Valyashko, V.M., 1990. Phase Equilibria and Properties of Hydrothermal Systems Nauka, Moscow, USSR. 270 pp. (in Russian, with English Abstr.).

Vanko, D.A., Bonnin-Mosbah, M., Philippot, P., Roedder, E., Sutton, S.R., 2001. Fluid inclusions in quartz from oceanic hydrothermal specimens and the Bingham, Utah porphyry-Cu deposit: a study with PIXE and SXRF. Chem. Geol. 173, 227–238.

Wallace, P.J., 2002. Vapor saturation in felsic magmas & vapor–melt partitioning of sulfur. Abstracts Goldschmidt Conference (Davos), Geochim. Cosmochim. Acta 66 (15a), A818.

Webster, J.D., 1990. Partitioning of F between H_2O and CO_2 fluids and topaz rhyolite melt. Contrib. Mineral. Petrol. 104, 424–438.

Webster, J.D., 1997. Exsolution of magmatic volatile phases from Cl-enriched mineralizing granitic magmas and implications for ore metal transport. Geochim. Cosmochim. Acta 61, 1017–1029.

Webster, J.D., Rebbert, C.R., 2001. The geochemical signature of fluid-saturated magma determined from silicate melt inclusions in Ascension Island granite xenoliths. Geochim. Cosmochim. Acta 65, 123–136.

Webster, J.D., Holloway, J.R., Hervig, R.L., 1989. Partitioning of lithophile trace elements between H_2O and H_2O+CO_2 fluids and topaz rhyolite melt. Econ. Geol. 84, 116–133.

Wood, S.A., 1992. Theoretical prediction of speciation and solubility of beryllium in hydrothermal solutions to 300 °C at saturated vapor pressure: application to bertrandite/phenakite deposits. Ore Geol. Rev. 7, 249–278.

Yarmolyuk, V.V., Litvinovsky, B.A., Kovalenko, V.I., Jahn, B.M., Zanvilevich, A.N., Vorontsov, A.A., Zhuravlev, D.Z., Posokhov, V.F., Kuz'min, D.V., Sandimirova, G.P., 2001. Stages of formation and sources of the peralkaline granitoid magmatism of the Northern Mongolia–Transbaikalia Rift Belt during the Permain and Triassic. Petrology 9, 302–328.

Zanvilevich, A.N., Litvinovsky, B.A., Andreev, G.V., 1985. Mongolian–Transbaikalian Province of Alkaline and Peralkaline Granitoids Nauka, Moscow, USSR. 320 pp. (in Russian).